UNIVERSIDADE FEDERAL DE ALAGOAS
INSTITUTO DE FÍSICA
PÓS-GRADUAÇÃO EM FÍSICA DA MATÉRIA CONDENSADA

Theoretical Analysis of the difference-frequency generation in nonlinear Rayleigh scattering of acoustic beams

Anderson Bandeira de Melo

Maceió, Alagoas – Brasil

June – 2011

ANDERSON BANDEIRA DE MELO

Theoretical Analysis of the difference-frequency generation in nonlinear Rayleigh scattering of acoustic beams

Dissertation presented to the to the Instituto de Física of Universidade Federal de Alagoas. requirement for achieve a Masters degree in science.

Advisor: Prof. Dr. Glauber T. Silva

Maceió, Alagoas – Brasil

June – 2011

Catalogação na fonte
Universidade Federal de Alagoas
Biblioteca Central
Divisão de Tratamento Técnico
Bibliotecária Responsável: Valter dos Santos Andrade

M528t Melo, Anderson Bandeira de.
Theoretical analysis of the difference – frequency generation in nonlinear Rayleigh seattering of acoustic beams / Anderson Bandeira de Melo. – Maceió, 2011.
53 f.

Orientador: Glauber José Ferreira Tomaz da Silva.
Dissertação (mestrado em Física da Matéria Condensada) – Universidade Federal de Alagoas. Instituto de Física. Maceió, 2014.

Bibliografia: f. 48-53.

1. Geração de diferença de frequência. 2. Espalhamento (Física).
3. Espalhamento de Rayleigh. 4. Espalhamento não-linear.I. Título.

CDU: 531.772

Universidade Federal de Alagoas
Instituto de Física
Programa de Pós Graduação em Física

BR 104 km 14. Campus A.C. Simões
Cidade Universitária
Tabuleiro dos Martins
57072-970 Maceió - AL. Brasil
FONE : (82) 3214-1423/FAX 3214-1645

PARECER DA BANCA EXAMINADORA DE DEFESA DE DISSERTAÇÃO DE MESTRADO

"Theoretical analysis of the difference-frequency generation in nonlinear Rayleigh scattering of acoustic beams"

por

Anderson Bandeira de Melo

A Banca Examinadora composta pelos professores Glauber José Ferreira Tomaz da Silva (orientador), do Instituto de Física da Universidade Federal de Alagoas, Rodrigo de Paula Almeida Lima, do Instituto de Física da Universidade Federal de Alagoas e Antonio Adilton Carneiro, do Instituto de Física da USP/Ribeirão Preto, consideram o candidato aprovado com grau "A".

Maceió, 28 de junho de 2011

Prof Glauber José Ferreira Tomaz da Silva

Prof. Rodrigo de Paula Almeida Lima

Prof. Antonio Adilton Carneiro

I dedicate to my parents Marcina and Adalberto.

To Glauber, once an adivsor and now a great friend.

Acknowledgments

I would like to thank my parents Adalberto and Marcina for all the support, stimulus and comprehension during this journey.

I would like to thank my brother Marcinkus and my sister Milena.

I would like to thank my friends Juka, Butija, Piska, Valmiro, Dr. Samuel and Dra. Nallyanne for the good times.

I would like to thank my friends from the Instituto de Física Galo Cego, Neto, Fred, Golfinho, Paulo, Alex, Cabeça and Momba, for sharing time during the Master's work.

I would like to thank my friends Hermes, Baggio, Théo, José and Prof. Adilton for the great times in Ribeirão Preto and for helpful discussions.

I would like to thak the staff of the Instituto de Física Ester, Marcos, Bárbara, Nilda and D. Edileuza.

I would like to thank Dani for friendship and caring during this journey.

I would like to thank the Farid Mitri for helpful discussions and great times in Maceió.

I would like to thank my advisor Glauber T. Silva for dedication and patience.

I would like to thank FAPEAL and CAPES for sponsoring.

Abstract

In this work, the difference-frequency (DF) generation in the scattering of two acoustic waves by a sphere in the Rayleigh limit is theoretically analyzed. A multipole series is derived for the DF scattered pressure at the farfield by applying the method of successive approximation and the Green's function technique to the Westervelt's nonlinear wave equation. In the Rayleigh limit, this series has only the monopole, dipole, and quadrupole moments. These moments depend on the nonlinear interaction of the primary incident and scattered waves. Theoretical results are obtained for the case of two intersecting plane waves localized within a spherical spatial region. The radius of the interaction region is assumed to be much smaller than the distance from the scatterer to observation point (radial distance). A similar configuration is found in vibro-acoustography imaging system. The directive patterns of the DF scattered field are illustrated for plane waves intersecting at $0°, 45°, 90°$, and $180°$. The center- and differece-frequencies of the waves are 1.5 MHz and 50 kHz, respectively, while the spherical scatterer radius is 0.125 mm. These frequencies are typically used in vibro-acoustography. The behavior of the DF scattered pressure is also analyzed for two colinear plane waves with varying radial distance from the scatterer, center- and the difference-frequency. Results indicate that the interaction of the primary scattered waves is the main process behind difference-frequency generation for most parameter combinations chosen here. Based on this conclusion, we will also discuss the DF generation process in vibro-acoustography.

Keywords: Difference-frequency Generation, Rayleigh Scattering, Nonlinear Scattering.

Resumo

Neste trabalho, é analisado teoricamente a geração de diferença de frequência (DF) de duas ondas acústicas por uma esfera no limite de Rayleigh. Uma série de multipolos é derivada para a pressão espalhada da DF no campo distante aplicando o método de aproximações sucessivas e técnica de função de Green para a equação de onda não-linear de Westervelt. No limite de Rayleigh, a série contêm apenas momentos de monopolo, dipolo e quadrupolo. Estes momentos dependem da interação não-linear da onda primária incidente e das ondas espalhadas. Os resultados teóricos são obtidos para o caso de interseção de duas ondas planas localizadas dentro de uma região espacial esférica. O raio da região de interseção é assumido como sendo muito menor do que a distância a partir do espalhados para o ponto de observação (distância radial). Uma configuração similar ao encontrado no método de imageamento de vibro-acustografia. Os padrões diretivos do campo espalhado de DF são ilustrados para interseção de ondas planas a $0°, 45°, 90°$, e $180°$. A frequência-central e a DF são 1.5 MHz e 50 kHz, respectivamente, enquanto que o raio do espalhador é de 0.125 mm. Essas frequências são tipicamente usadas em vibro-acustografia. O comportamento da pressão espalhada de DF é também analisado para duas ondas planas colineares variando a distância radial a partir do espalhador, da frequência-central e DF. Os resultados indicam que a interação das ondas primárias espalhadas é o principal processo que explica a geração de diferença de frequeência para a maioria das combinações escolhidas neste trabalho. Baseado nesta conclusão, também é discutida o processo de geração de DF em vibro-acustografia.

Palavras-chave: Geração de Diferença de Frequência, Espalhamento de Rayleigh, Espalhamento não-linear.

List of Figures

Contents

Chapter 1

INTRODUCTION

1.1 Historical Background

Although nonlinear acoustics have considerably evolved in the last 40 years, the scientific investigation of this field dates back as early as 1750s[1]. The nonlinear wave equation for finite-amplitude in fluids was developed nearly at the same time as the linear wave equation for infinitesimal amplitude signals. In the first 200 years progress was not so fast. Two main reasons may explain this fact. Primarily, the ordinary linear acoustic does an outstanding job in explaining several acoustical phenomena. Second, the mathematical machinery necessary to tackle nonlinear wave propagation problems has been a very difficult lock to pick.

Over the past fifty years, nonlinear acoustics has developed into a vigorous and distinctive branch of science with several applications to technology[2]. The subject covers a wide range of topics, including steady finite amplitude waves in supersonic aerodynamics[3], weak shock theory[4], bubble dynamics and cavitation in liquids[5]. The practical applications are increasing: the nonlinear parametric

array devised by Westervelt[6] for the production of a highly directional low-frequency beam in water or air; the use of ultrasonics in biomedical imaging[7] and engineering nondestructive testing[8].

1.2 Difference-frequency Generation

The nonlinear combination of harmonic waves of distinct frequencies gives rise to secondary waves at higher harmonics as well as the sum- and difference- frequency components. The difference-frequency generation (DFG) in acoustics is a well known phenomena since the 18th century[9]. When two plane waves (primary) of finite amplitude are superimposed in space, they generate a difference frequency wave whose amplitude is proportional to the distance from the wavefront to the acoustic source[10]. This phenomenon is knows as "scattering of sound by sound"[11]. When the primary waves propagate in the same direction, the DFG is known as parametric array effect.

In 1963, Westervelt proposed a theoretical framework where two high-frequency and highly collimated sound beam interact nonlinearly generating the difference-, sum-frequency and high order harmonics of the primary waves. He does proposed the concept of the parametric acoustic array[6]. The applications of parametric arrays are seen in underwater acoustics[12], nonlinear acoustic tomography[13], and audiospotlight[14]. This generation happens because the incident and scattered primary waves interact nonlinearly throughout the space up to the observation point. Another application of the DFG is found in some acoustical imaging methods such as nonlinear parameter tomography[15,16] and vibro-acoustography[17,18].

Vibro-acoustography imaging method represents a new application of the DFG. This method employs two tightly focused ultrasound beams (in MHz range). The frequency of the beams are slightly different (in kHz range). The DFG in the beams interaction process within biological tissue is used to form an image of the region of interest. The difference-frequency signal from the focal zone is acquired by a sensitive acoustic detector which is recorded and processed to synthesize the image. The interaction process might be influenced by the nonlinear interaction of the primary scattered waves due the presence of the inhomogeneities in the medium.

1.3 Rayleigh Scattering

In the presence of an inclusion, the DFG might be enhanced by two mechanisms. Firstly, incident waves will produce a radiation force by linear and nonlinear interactions with the inclusion[19,20]. In turn, the inclusion is set in motion emitting waves whose frequencies correspond to the components present in the dynamic force. Secondly, the primary waves (incident and scattered) associated to the fundamental frequencies will interact between themselves yielding secondary waves.

When the scatterer target is much smaller than the incident wavelengths, the scattering problem approaches to the Rayleigh limit. This kind of scattering is a well-known phenomenon in Electromagnetics[21], which has been subjected to considerable study for more than a Century. Lord Rayleigh developed the concept of scattering[22] and his contributions in this area provided the foundation of which almost all subsequent work is based[23,24]. In our work, the theoretical framework presented to the difference-frequency generation is analyzed as nonlinear acoustic

scattering by ultrasound beams upon a small sphere, i. e., the Rayleigh limit.

1.4 Motivation

The role of the DFG seems to have been underestimated in vibro-acoustography[25]. This gave us the stimulus to theoretically investigate the DFG in acoustic scattering. With this motivation, we perform an analysis of nonlinear acoustic scattering by a small sphere (Rayleigh limit). This problem has not yet been investigated before. So far, difference frequency generation in scattering process can be divided into two categories. In the scattering by a moving target[26,27], the difference-frequency takes place due to the interaction of the incident wave with the radiation caused by the vibration (breathing mode) of the scatterer. In contrast, two or more incident plane waves scattered by a fixed target may produce difference-frequency waves as the incident and scattered waves nonlinearly interact[28,29].

1.5 Purpose of this work

Our study aims at obtaining the solution of the DFG in the scattering of two plane waves by a small sphere. The difference-frequency pressure is obtained solving the Westervelt nonlinear wave equation[6] through the method of successive approximations along with the Green's function technique. The primary incident and scattered pressures are represented through the partial wave expansion in spherical coordinates. In the Rayleigh limit, the difference-frequency scattered wave is expressed by a multipole series, which has only a monopole, dipole and quadrupole moments. The directive pattern of the scattered pressure is analyzed for two plane waves inter-

secting at the following angles at 0^0, 45^0, 90^0 and 180^0. The incident waves interact within a spherical region whose radius is assumed to be much smaller than the radial distance to the scatterer. A special attention is drawn for the scattering of two collinear plane waves. Different arrangements with varying parameters such as radial distance to the spherical scatterer, center- and difference-frequency are considered. The center- and the difference-frequency are chosen within $0.5 \sim 1.5$MHz and $10 \sim 300$kHz, respectively.

1.6 List of Publications

1.6.1 Conferences

- XVI Congresso Brasileiro de Física Médica. *Vibro-acustografia de Multifrequência Baseada em Harmônicos de Diferença de frequência.* São Paulo–SP, 2009.

- XI Latin American Workshop on Nonlinear Phenomena. *Difference-frequency Generation in Nonlinear Acoustics.* Búzios–RJ, 2009.

- XXXIII Encontro Nacional de Física da Matéria Condensada. Spectral analysis of multiple difference-frequency generation in nonlinear acoustics. Águas de Lindóia–SP, 2010.

1.6.2 Articles

- A. Bandeira, G. T. Silva. *Difference-frequency generation in nonlinear scattering of acoustic waves by a rigid sphere.* Ultrasonics. *Published*

Chapter 2

NONLINEAR WAVE PROPAGATION

When two finite amplitude sound waves interact in a fluid, the phenomenon of generation of sound waves occurs. The frequencies of these generated sound beams corresponds to the sum and difference frequency of the primary waves. This phenomenon is well known as "nonlinear interaction of sound waves" or the "scattering of sound by sound"[14]. Taking account the Lighthill's arbitrary fluid dynamics equation[30], Westervelt derived a second order inhomogeneous wave equation[6] which is satisfied by the with nonlinear interaction. The present work is based on the Westervelt equation due its description of the nonlinear wave motion in a homogeneous fluid.

In sec. 2.1 we present the characteristics of our fluid and take a brief derivation of the Westervelt equation. Treating the fluid as weakly nonlinear, in sec. 2.2, we take the secondary generated field as a perturbation and split the equation into a system of linear wave equations using the method of successive approximations.

2.1 Westervelt Equation

Let us consider a weakly thermoviscous and homogeneous fluid at rest. The wave dynamics in the fluid is characterized as the excess of pressure p and the particle velocity $\mathbf{v} = -\nabla\phi$ with ϕ being the potential function. These fields are functions of the position vector $\mathbf{r}$ and the time t. The steady state of the fluid represents the ambient density as ρ_0, pressure p_0 and $\mathbf{v} = 0$. The excess of pressure is given in terms of the potential function as[31]

$$p = \rho_0 \frac{\partial \phi}{\partial t} - \mathcal{L} \tag{2.1}$$

where $\mathcal{L}$ is the second-order Lagrangian density for the wave motion given by

$$\mathcal{L} = \frac{1}{2}\rho_0 v^2 - \frac{p^2}{2\rho_0 c_0^2} = \frac{\rho_0}{4}\Box^2\phi^2 \tag{2.2}$$

which appears as a natural variable in the equations, the variable c_0 is the small amplitude speed of sound, $v^2 = \mathbf{v}\cdot\mathbf{v}$, and $\Box^2 = \nabla^2 - (1/c_0^2)(\partial/\partial t)^2$.

Starting from the basic equations, equation of motion and equation of continuity combined with the equations of state, can be written, respectively, in the second order approximation as[31]

$$\rho_0 \frac{\partial \mathbf{v}}{\partial t} + \nabla(p + \mathcal{L}) = 0, \quad \text{and} \tag{2.3}$$

$$\frac{\partial}{\partial t}(p + \mathcal{L}) + \rho_0 c_0^2 \nabla\cdot\mathbf{v} = \frac{\beta}{\rho_0 c_0^2}\frac{\partial}{\partial t}(p - p_0)^2 + 2\frac{\partial \mathcal{L}}{\partial t}. \tag{2.4}$$

The $\beta = 1 + B/2A$ is the nonlinear coefficient, with $B/2A = (\rho_0^2 c_0^2/2)(\partial^2 p/\partial\rho^2)$ being the fluid the nonlinear parameter[32]. The ratio B/A has become a common term in the field of nonlinear acoustics, which is originated from the Taylor series expansion of the equation of state, $p = p(\rho)$, up to the second order in $(\rho - \rho_0)$

$$p - p_0 = c_0^2(\rho - \rho_0) + \frac{1}{2}\left(\frac{\partial^2 p}{\partial \rho^2}\right)_{(\rho=\rho_0)}(\rho - \rho_0)^2 + \ldots \tag{2.5}$$

This parameter determines the relative importance of the leading finite-amplitude correction to the small-signal sound speed c_0.

The ordinary acoustic pressure field $p - p_0$ is in general, not governed by the Westelvet equation. Indeed, if we combine Eq. 2.3 and Eq. 2.4, we find

$$\Box^2 p = -\frac{\beta}{\rho_0 c_0^4}\frac{\partial^2}{\partial t^2}(p - p_0)^2 - \nabla^2 \mathcal{L} - \frac{1}{c_0^2}\frac{\partial^2 \mathcal{L}}{\partial t^2}. \tag{2.6}$$

However, in the farfield the last two terms approaches to zero, and then, the Eq. 2.6 becomes the Westervelt equation

$$\Box^2 p = -\frac{\beta}{\rho_0 c_0^4}\frac{\partial^2}{\partial t^2}(p - p_0)^2. \tag{2.7}$$

This equation accounts for the diffraction as well as the medium nonlinearity in the wave propagation. Thermoviscous effects are neglected in our analysis. It is worthy to remark that Eq. 2.7 is valid when cummulative nonlinear effects (such as wave distortion) are more prominent that local properties of the acoustic field near to the acoustic source. When the wave propagates near to the scatterer, the wave pressure which satisfies Eq. 2.7 should be mofified to[1]

$$\tilde{p} = p + \frac{\rho_0}{4}\left(\nabla^2 - \frac{1}{c_0^2}\frac{\partial^2}{\partial t^2}\right)\phi^2. \tag{2.8}$$

Due the fact that we want to describe the difference-frequency scattered wave in the farfield only, Eq. 2.7 suffices to model the nonlinear wave propagation. For further discussion the reader may refer to Mark and David[1].

2.2 Method of Successive Approximations

Assuming that the wave propagates in the medium with pressure magnitude given in terms of the Mach number $\varepsilon = v_0/c_0$, where v_0 is the maximum magnitude of

the particle velocity. The Westervelt equation Eq. 2.7 can be reduced to a set of hierarchical linear wave equations through the method of successive approximation. We can expand the pressure up to the second-order as follows

$$p = \varepsilon p^{(1)} + \varepsilon^2 p^{(2)} \tag{2.9}$$

where $p^{(1)}$ is the linear solution (first-order approximation) of the Westervelt equation and $p^{(2)}$ is a small correction to $p^{(1)}$ (second-order approximation, for $|p^{(2)}| \ll |p^{(1)}|$ throughout the nonlinear interaction region). By substituing Eq. 2.9 in Eq. 2.7 and equating powers like of ε and ε^2, we obtain

$$\left(\nabla^2 - \frac{1}{c_0^2}\frac{\partial}{\partial t^2}\right)p^{(1)} = 0, \tag{2.10}$$

$$\left(\nabla^2 - \frac{1}{c_0^2}\frac{\partial}{\partial t^2}\right)p^{(2)} = -\frac{\beta}{\rho_0 c_0^4}\frac{\partial^2 p^{(1)2}}{\partial t^2}. \tag{2.11}$$

These equations form a set of linear hierarchical wave equations. They describe the dynamics of weak amplitude waves.

Chapter 3

SCATTERING THEORY

In this chapter our attention turns to the scattering theory of acoustic waves. In Sec. 3.1, we derive the solution for the spherical wave equation as a partial wave expansion of the pressure. This series representation of the pressure field is important for us because it behaves as a general solution for any kind of objects which occupy a finite volume in space.

In the Sec. 3.2 we present the incident and the scattered field expressed both in terms of partial wave expansions. We also present, in Sec. 3.3, how to find the solution for the difference-frequency generation with the Green's function machinery. As we previously established, the scattering problem is restricted to the Rayleigh limit, which will be also discussed here, in Sec. 3.7. As an application to this theory, we present in Sec. 3.8 the theoretical issues of the vibro-acoustography imaging method.

3.1 Partial Wave Expansion

In spherical coordinates, we have the time-dependent wave equation which is expressed as

$$\frac{1}{r^2}\frac{\partial}{\partial r}\left(r^2\frac{\partial p}{\partial r}\right)+\frac{1}{r^2\sin\theta}\frac{\partial}{\partial\theta}\left(\sin\theta\frac{\partial p}{\partial\theta}\right)+\frac{1}{r^2\sin\theta^2}\frac{\partial^2 p}{\partial\phi^2}-\frac{1}{c^2}\frac{\partial^2 p}{\partial t^2}=0. \tag{3.1}$$

One of the way to obtain the solution of this equation is using the method of separation of variables for which

$$p(r,\theta,\phi,t)=R(r)\Theta(\theta)\Phi(\phi)T(t). \tag{3.2}$$

Substituting this equation into Eq. 3.1 yields the following system of ordinary differential equations

$$\begin{cases}\dfrac{d^2\Phi}{d\phi^2}+m^2\Phi=0\\ \dfrac{1}{\sin\theta}\dfrac{d}{d\theta}\left(\sin\theta\dfrac{d\Theta}{d\theta}\right)+\left[l(l+1)-\dfrac{m^2}{\sin^2\theta}\right]\Theta=0\\ \dfrac{1}{r^2}\dfrac{d}{dr}\left(r^2\dfrac{dR}{dr}\right)+k^2R^2-\dfrac{l(l+1)R}{r^2}=0\\ \dfrac{1}{c^2}\dfrac{d^2T}{dt^2}+k^2T=0\end{cases} \tag{3.3}$$

The solution for the angular equations can be combined into a single function called spherical harmonics defined by

$$Y_l^m(\theta,\phi)\equiv\sqrt{\frac{(2l+1)}{4\pi}\frac{(l-m)!}{(l+m)!}}P_l^m(\cos\theta)e^{im\theta} \tag{3.4}$$

where m and l are integers and $P_l^m(\cos\theta)$ is the Legendre function, with $|m|<l$ and $l>0$. For the radial part, the solutions can be written as

$$R(r)=R'j_l(kr)+R''y_l(kr) \tag{3.5}$$

where $j_l(kr)$ and $y_l(kr)$ are spherical Bessel functions of the first and second kind, respectively, and R' and R'' are complex constants. Alternatively, this solution can be written as

$$R(r) = R'''h_l^{(1)}(kr) + R''''h_l^{(2)}(kr) \tag{3.6}$$

where $h_l^{(1)}(kr)$ and $h_l^{(2)}(kr)$ are spherical Hankel functions of the first and second kind, respectively, and R''' and R'''', are complex constants.

Thus, we can write the solution of Eq. 3.1, in the absence of time, as a partial wave expansion

$$p(r,\theta,\phi,\omega) = \sum_{l=0}^{\infty}\sum_{m=-l}^{l}[A_{ml}j_l(kr)]Y_l^m(\theta,\phi) \tag{3.7}$$

for a interior problem general solution[33], see Fig. 3.1 and

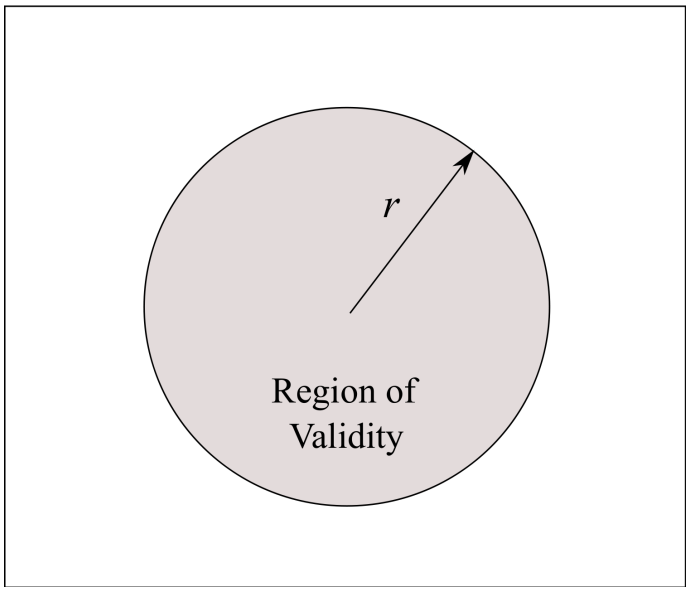

Figure 3.1: The grey area represents the region of validity for the interior solution.

$$p(r,\theta,\phi,\omega) = \sum_{l=0}^{\infty}\sum_{m=-l}^{l}[B_{ml}h_l^{(1)}(kr)]Y_l^m(\theta,\phi) \tag{3.8}$$

for a exterior problem general solutions[33], see Fig. 3.2. The A_{ml}, B_{ml} are complex

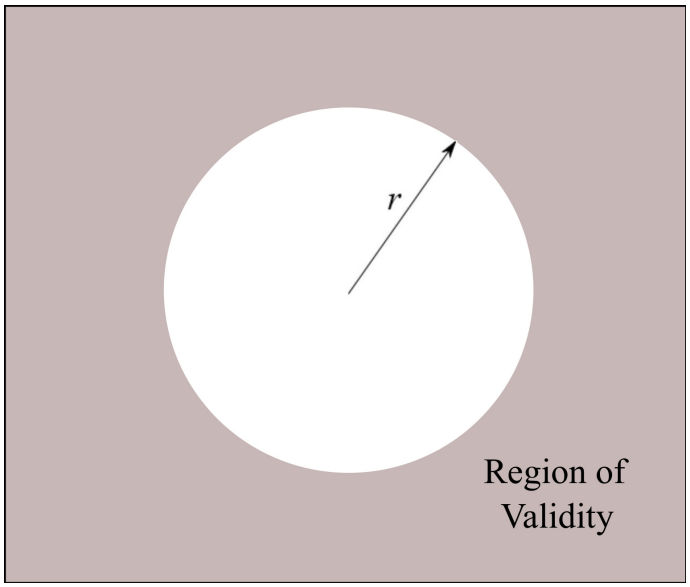

Figure 3.2: The grey area represents the region of validity for the exterior solution.

constants which can be found as

$$A_{ml} = \frac{1}{j_l(kb)} \int_{4\pi} p(b,\theta,\phi) Y_l^{m*}(\theta,\phi) \sin\theta d\Omega, \tag{3.9}$$

and,

$$B_{ml} = \frac{1}{h_l(kb)} \int_{4\pi} p(b,\theta,\phi) Y_l^{m*}(\theta,\phi) \sin\theta d\Omega, \tag{3.10}$$

respectively. The importance of the partial wave expansion lies on the fact that any function on an arbitrary shape of finite volume can be expanded in terms of them.

3.2 Linear scattering

Let us assume now that two primary acoustic beams at frequencies ω_2 and ω_1 propagate in the medium considered in the Chap. 2. We consider that $\omega_2 > \omega_1$. The pressure field of the incident beam is given by

$$p_{\mathrm{I}} = \varepsilon \rho_0 c_0^2 (\hat{p}_{\mathrm{I},1} e^{-i\omega_1 t} + \hat{p}_{\mathrm{I},2} e^{-i\omega_2 t}), \tag{3.11}$$

where $\hat{p}_{\mathrm{I},1}$ and $\hat{p}_{\mathrm{I},2}$ are the dimensionless amplitudes of the acoustic beams. In terms of the partial wave expansion, we have

$$\hat{p}_{\mathrm{I},n} = \sum_{l,m} a_{n,l}^{m} j_l(k_n r) Y_l^m(\theta, \phi), \quad n = 1, 2 \tag{3.12}$$

where $\sum_{l,m} \to \sum_{l=0}^{\infty} \sum_{m=-l}^{l}$, $\{a_{n,l}^{m}\}$ are the beam shape coefficients to be determined depending on the type of acoustic wave considered.

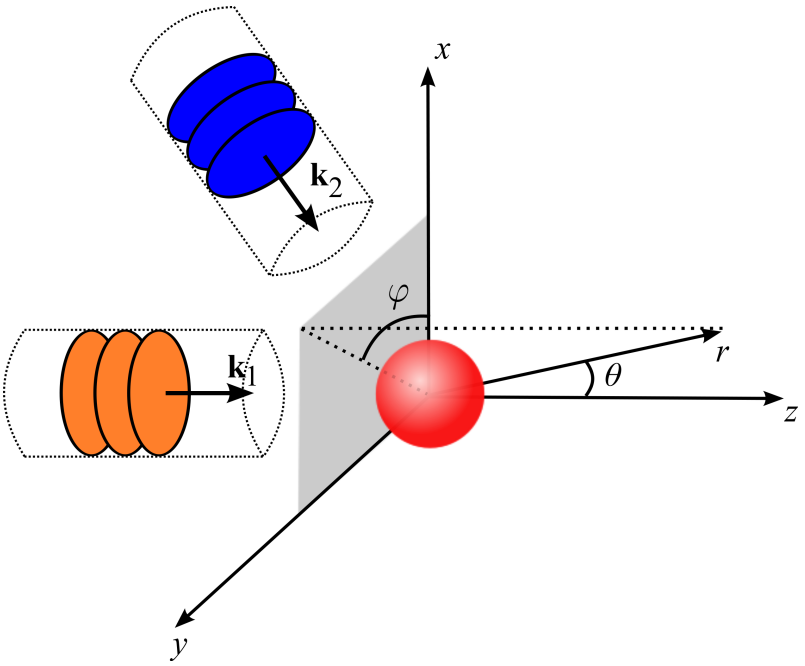

Figure 3.3: Outline of the scattering problem. Two waves with wavevectors $\mathbf{k}_1$ and $\mathbf{k}_2$ insonify a rigid sphere of radius a. The sphere is placed at the center of the coordinate system. The observation point of the scattered pressure, in spherical coordinates, is $\mathbf{r} = (r, \theta, \varphi)$.

Considering that a rigid sphere of radius a is placed in the wavepath. The origin of the coordinate system is set at the center of the spherical scatterer, see Fig. 3.3. In this configuration, the beam shape for the incident beam can be found

as

$$a_{n,l}^{m} = \frac{1}{j_l(ka)} \int_{4\pi} \hat{p}_{\mathrm{I},n}(a,\theta,\phi) Y_l^{m*}(\theta,\phi) d\Omega, \quad n = 1,2. \tag{3.13}$$

When two primary waves interact with the scatterer, linear scattered waves appear in the medium. Thus, the pressure field of the scattered beam is given by

$$p_{\mathrm{S}} = \varepsilon \rho_0 c_0^2 (\hat{p}_{\mathrm{S},1} e^{-i\omega_1 t} + \hat{p}_{\mathrm{S},2} e^{-i\omega_2 t}), \tag{3.14}$$

where $\hat{p}_{\mathrm{S},1}$ and $\hat{p}_{\mathrm{S},2}$ are the amplitude of the scattered pressure is then given in terms of the multipole expansion as follows

$$\hat{p}_{\mathrm{S},n} = \sum_{l,m} s_{n,l}^{m} h_l^{(1)}(k_n r) Y_l^m(\theta,\phi), \quad n = 1,2 \tag{3.15}$$

where $\{s_{n,l}^{m}\}$ are the scattering coefficients for each linear incident wave. When we substitute Eqs. 3.11 and 3.14 into the first order Westervelt equation, Eq. 2.10, we see that the pressure amplitudes satisfy the Helmholtz equation

$$(\nabla^2 + k_n^2) \begin{pmatrix} \hat{p}_{\mathrm{I},n} \\ \\ \hat{p}_{\mathrm{S},n} \end{pmatrix} = 0, \quad n = 1,2, \tag{3.16}$$

The scattered pressure should also satisfy the Sommerfeld radiation condition. The boundary condition for the rigid sphere requires that the particle velocity vanish of the sphere surface. It means that, in terms of pressure, this condition corresponds to the Neumann boundary condition. Equating this

$$\left[\frac{\partial (\hat{p}_{\mathrm{I},n} + \hat{p}_{\mathrm{S},n})}{\partial r} \right]_{r=a} = 0. \tag{3.17}$$

And from the boundary in Eq. 3.17, we obtain the scattering coefficients as

$$s_{n,l}^{m} = -\frac{j_l'(k_n a)}{h_l'^{(1)}(k_n a)} a_{n,l}^{m}, \quad n = 1,2, \tag{3.18}$$

where the prime symbol means derivation.

3.3 Difference-frequency generation

The primary incident and scattered waves interact nonlinearly in a region exterior of the scatterer and the sum- and difference-frequency waves are generated. However, for our purpose, we are only interested on the difference-frequency generation. Thus, according to Eq. 2.9, the difference-frequency scattered pressure is written as a second order field

$$p_- = \varepsilon \rho_0 c_0^2 \hat{p}_- e^{-i\omega_- t}, \tag{3.19}$$

where $\hat{p}_-$ is the dimensionless pressure amplitude. Substituting Eq. 3.19 into Eq. 2.11 we find that the difference-frequency pressure amplitude satisfies the inhomogeneous Helmholtz equation

$$(\nabla^2 + k_-^2)\hat{p}_- = \beta k_-^2 \mathcal{P}, \tag{3.20}$$

where

$$\mathcal{P} = \hat{p}_{1,I}^* \hat{p}_{2,S} + \hat{p}_{1,I}^* \hat{p}_{2,S} + \hat{p}_{1,S}^* \hat{p}_{1,I} + \hat{p}_{1,S}^* \hat{p}_{2,S}. \tag{3.21}$$

The source term $\mathcal{P}$ has all possible interactions between the primary and incident waves.

3.4 Boundary Conditions

The uniqueness of the solutions of Eqs. 3.16 and 3.20 depend on the problem's boundary conditions. For a rigid and immovable sphere, the boundary conditions requires that the normal component of the particle velocity vanish on the sphere's surface. At the infinity the pressure amplitudes should satisfy the Sommerfeld radiation condition.

The particle velocity given up to the second-order approximation is expressed as

$$\mathbf{v} = \varepsilon \mathbf{v}^{(1)} + \varepsilon^2 \mathbf{v}^{(1)}, \quad \varepsilon \ll 1, \tag{3.22}$$

where $\mathbf{v}^{(1)}$ and $\mathbf{v}^{(2)}$ are the linear and the second-order velocity fields, respectively. Thus, for the linear velocity we have $\mathbf{v}^{(1)} \cdot \mathbf{e}_r|_{r=a} = 0$, where $\mathbf{e}_r$ is the outward normal unit-vector to the sphere. From the linear momentum conservation equation $\rho_0(\partial \mathbf{v}^{(1)}/\partial t) = -\nabla p^{(1)}$, we find the following condition for the pressure

$$\left[\frac{\partial(\hat{p}_{\mathrm{I},n} + \hat{p}_{\mathrm{S},n})}{\partial r}\right]_{r=a} = 0. \tag{3.23}$$

After substituting Eqs. 3.12 and 3.13 into last equation, we obtain the scattering coefficients as $s_{n,l}^m = s_{n,l} a_{n,l}^m$, where

$$s_{n,l} = -\frac{j_l'(k_n a)}{h_l'^{(1)}(k_n a)}, \quad n = 1, 2, \tag{3.24}$$

with the prime symbol meaning derivation.

The second-order particle velocity satisfies the conservation equation, given in Eq. 2.3. Projecting this equation onto $\mathbf{e}_r$ at the sphere's surface, we obtain

$$\left.\frac{\partial p^{(2)}}{\partial r}\right|_{r=a} = -\left.\frac{\partial \mathcal{L}}{\partial r}\right|_{r=a}. \tag{3.25}$$

Now, using the linear relation $p^{(1)} = \rho_0(\partial \phi^{(1)}/\partial t)$ and Eqs. 2.8 and 3.25, we find the difference-frequency boundary condition as

$$\left.\frac{\partial \hat{p}_-}{\partial r}\right|_{r=a} = -\frac{k_-^2}{2k_1 k_2}\left.\frac{\partial \mathcal{P}}{\partial r}\right|_{r=a}. \tag{3.26}$$

3.5 Green's function solution

The solution of Eq. 3.20 can be obtained through the Green's function method. Due the fact that the normal derivative of the difference-frequency pressure is specified

on the sphere's surface, the normal derivative of the Green's function on this surface should vanish. Thereby, the difference-frequency pressure amplitude given in terms of the Green's function $G(\mathbf{r}|\mathbf{r'})$ reads (morse-ingard)

$$\begin{aligned} \hat{p}_- &= -\beta k_-^2 \left[\int_V \mathcal{P}(\mathbf{r'}) G(\mathbf{r}|\mathbf{r'}) dV' \right. \\ &+ \left. \int_S \left(\frac{\partial \hat{p}_-}{\partial r'} \right)_{r'=a} G(\mathbf{r}|\mathbf{r'}) dS' \right], \quad k_- r \gg 1, \end{aligned} \tag{3.27}$$

where S denotes the sphere's surface and V is the volume of the spatial region from S to infinity.

The contribution of the surface integral for two interacting spherical waves (monopoles) is found to be $k_-^3/(k_1 k_2)^2$ in Appedix A (fazer). In contrast, it will be shown that the magnitude of the volume integral in Eq. 3.27 is proportional to $\beta k_-/(k_1 k_2)$. Thus, the ratio of the volume to the surface integral is $k_-^2/(k_1 k_2)$. It is convinient to write the primay angular frequencies in a symmetric way as follows $\omega_1 = \omega_0 - \omega_-/2$ and $\omega_2 = \omega_0 + \omega_-/2$, where ω_0 is the mean frequency. Now the ratio between the integrals can be expressed as $\beta^{-1}[(\omega_0/\omega_-)^2 - 1/4]^{-1}$. Note that ω_0/ω_- is the downshift ratio. If the contribution from the surface integral is about 0.01 of that from the volume integral in water, the downshift ratio should be larger than 5. Therefore, limiting our analysis to downshift ratios larger than 5, we can neglect the surface integral in Eq. (20).

The volume integral can be split into two regions: $a \leq r' < r$ (inner source volume) and $r < r'$ (outer source volume). In Appendix B, the integral for the outer volume is estimated for two interacting spherical waves. The result shows that this integral is $O(r^{-2})$. It will be demonstrated that the inner volume integral evaluated in the farfield is $O(r^{-1})$. Therefore, the outer volume integral can be neglected in

the farfield. Therefore, the difference-frequency pressure amplitudes becomes

$$\hat{p}_-(\mathbf{r}) = -\beta k_-^2 \int_a^r \int_{4\pi} \mathcal{P}(\mathbf{r'}) G(\mathbf{r}|\mathbf{r'}) r'^2 dr' d\Omega', \tag{3.28}$$

where $d\Omega'$ is the infinitesimal solid angle. The Green's function in the region $r' < r$, which satisfies the Neumann boundary condition on the sphere surface, is given by (morse ingard)

$$\begin{aligned} G &= ik_- \sum_{l,m} \left[j_l(k_- r') - \frac{j_l'(k_- a)}{h_l'^{(1)}(k_- a)} h_l'^{(1)}(k_- r') \right] Y_l^{m*}(\theta', \phi') \\ &\times \; h_l^{(1)}(k_- r) Y_l^m(\theta, \phi) \end{aligned} \tag{3.29}$$

The difference-frequency generation is analyzed in the limit where $k_- a \ll 1$. Using the asymptotic formulas of the spherical functions for small argument[34], it can be shown that the lowest terms are

$$\frac{j_0'(k_- a)}{h_0'^{(1)}(k_- a)} \sim \frac{i(k_- a)^3}{3}, \tag{3.30}$$

$$\frac{j_1'(k_- a)}{h_1'^{(1)}(k_- a)} \sim -\frac{i(k_- a)^3}{6}, \quad k_- a \ll 1. \tag{3.31}$$

Based on these results, the second term inside the brackets in Eq.3.29 can be neglected when $k_- a \ll 1$, and our Green's function can be reduced to

$$G = ik_- \sum_{l,m} j_l(k_- r') Y_l^{m*}(\theta', \phi') h_l^{(1)}(k_- r) Y_l^m(\theta, \phi). \tag{3.32}$$

We are now prepared to obtain the difference-frequency scattered pressure. In Eq. 3.32 we use the asymptotic expression of the spherical Hankel function for large argument[34]. Thus, if we substitute Eq. 3.21 and Eq. 3.32 into Eq. 3.28, we can express the difference-frequency scattered pressure at the farfield as

$$\hat{p}_-(r, \theta, \phi) = \frac{\beta k_- f(r, \theta, \phi)}{k_1 k_2} \frac{e^{ik_- r}}{r}. \tag{3.33}$$

The function f is named the scattering form function at the difference-frequency and is given by

$$f_-(r,\theta,\phi) = \sum_{l,m} S_l^m(r) Y_l^m(\theta,\phi) \tag{3.34}$$

is the difference-frequency form function. The interaction function is expressed as

$$\begin{aligned} S_l^m &= -i^{-l} \sum_{l_1,m_1} \sum_{l_2,m_2} \sqrt{\frac{(2l_1+1)(2l_2+1)}{4\pi(2l+1)}} \\ &\times C^{l,0}_{l_1,0,l_2,0} C^{l,m}_{l_1,m_1,l_2,m_2} a^{m_1*}_{1,l_1} a^{m_2}_{2,l_2} \\ &\times (\varrho^{(\mathrm{II})}_{l_1 l_2 l} + s^*_{1,l_1} \varrho^{(\mathrm{SI})}_{l_1 l_2 l} + s^*_{2,l_2} \varrho^{(\mathrm{IS})}_{l_1 l_2 l} + s^*_{1,l_1} s_{2,l_2} \varrho^{(\mathrm{SS})}_{l_1 l_2 l}) \end{aligned} \tag{3.35}$$

where $\{C^{l,m}_{l_1,m_1,l_2,m_2}\}$ are the Clebsch-Gordan coefficients, which come from the angular integration[35]

$$\begin{aligned} \int_{4\pi} Y_{l_1}^{m_1*} Y_{l_2}^{m_2} Y_l^m d\Omega &= (-1)^{-m_1} \sqrt{\frac{(2l_1+1)(2l_2+1)}{4\pi(2l+1)}} \\ &\times C^{l,0}_{l_1,0,l_2,0} C^{l,-m}_{l_1,-m_1,l_2,m_2} \end{aligned} \tag{3.36}$$

The Clebsch-Gordan coefficient should satisfy the following conditions[36]

$$\begin{aligned} m_1 + m_2 &= m, \\ |l_2 - l_1| \leq l &\leq l_2 + l_1, \end{aligned} \tag{3.37}$$

otherwise it values are zero. Furthermore, when $m_1 = m_2 = m = 0$ the sum l_1+l_2+l should be even or the coefficient becomes zero. The radial function in the scattering form function, Eq. 3.34, is

$$\begin{aligned} \mathcal{R}^{m_1 m_2 m}_{l_1 l_2 l} &= a^{m_1*}_{1,l_1} a^{m_2}_{2,l_2} \varrho^{(\mathrm{II})}_{l_1 l_2 l} + s^{m_1*}_{1,l_1} a^{m_2}_{2,l_2} \varrho^{(\mathrm{SI})}_{l_1 l_2 l} \\ &+ a^{m_1*}_{1,l_1} s^{m_2}_{2,l_2} \varrho^{(\mathrm{IS})}_{l_1 l_2 l} + s^{m_1*}_{1,l_1} s^{m_2}_{2,l_2} \varrho^{(\mathrm{SS})}_{l_1 l_2 l} \end{aligned} \tag{3.38}$$

where the function $\varrho^{(\cdot\cdot)}$ stands for each possible interaction, i.e. incident-with-incident (II), scattered-with-incident (SI), incident-with-scattered (IS) and scattered-

with-scattered (SS). These functions are given by the relations

$$\varrho^{(\mathrm{II})}_{l_1 l_2 l} = k_1 k_2 k \int_a^r j_l(k_- r') j_{l_1}(k_1 r') j_{l_2}(k_2 r') dr', \tag{3.39}$$

$$\varrho^{(\mathrm{IS})}_{l_1 l_2 l} = k_1 k_2 k \int_a^r j_l(k_- r') j_{l_1}(k_1 r') h^{(1)}_{l_2}(k_2 r') dr', \tag{3.40}$$

$$\varrho^{(\mathrm{SI})}_{l_1 l_2 l} = k_1 k_2 k \int_a^r j_l(k_- r') h^{(2)}_{l_1}(k_1 r') j_{l_2}(k_2 r') dr', \tag{3.41}$$

$$\varrho^{(\mathrm{SS})}_{l_1 l_2 l} = k_1 k_2 k \int_a^r j_l(k_- r') h^{(2)}_{l_1}(k_1 r') h^{(1)}_{l_2}(k_2 r') dr', \tag{3.42}$$

The integrals in Eqs. 3.39–3.42 were calculated with Mathematica software[37] for $l = 0, 1, 2$ and $l_1 = l_2 = 0, 1$, for the Rayleigh limit.

We now present the results for two radial integrals $\varrho^{(\mathrm{SS})}_{011}$ and $\varrho^{(\mathrm{SI})}_{000}$ to illustrate the method we used here, which is based on Mathematica software.

```
SS[r_,0,1,1]:= Integrate[x^2 * SphericalBesselJ[0,(k_2 - k_1) * x] *
SphericalHankelH2[1,k_1*x] * SphericalHankelH1[1,k_2*x], {x,a,r},
Assumptions → k_1 > 0 && k_2 && k_1 && a > 0 && r > a ]
```

Figure 3.4: Command line to calculate the integral $\varrho^{(\mathrm{SS})}_{011}$

```
SI[r_,0,0,0]:= Integrate[x^2 * SphericalBesselJ[0,(k_2 - k_1) * x] *
SphericalBesselJ[0,k_1*x] * SphericalHankelH1[0,k_2*x], {x,a,r},
Assumptions → k_1 > 0 && k_2 && k_1 && a > 0 && r > a ]
```

Figure 3.5: Command line to calculate the integral $\varrho^{(\mathrm{SI})}_{000}$

In Figs. 3.4 and 3.5 the command line of the input code are shown, respectively. Their results with some simplifications are demonstrated as

$$\begin{aligned}\varrho_{011}^{(\mathrm{SS})} &= \frac{k_-^2}{4k_1^2k_2^2a^2}\Big\{i - ie^{2ik_-a} + a[2k_2 - k_1(2+5\pi k_2 a)] + 2ik_1k_2a^2 \\ &\times \left[\mathrm{Ei}(2ik_-a) - \mathrm{Ei}(2ik_-r) + \ln\left(\frac{r}{a}\right) - \frac{\pi}{4i}\right]\Big\},\end{aligned} \tag{3.43}$$

and

$$\begin{aligned}\varrho_{000}^{(\mathrm{SI})} &= \frac{ik_-^2}{4k_1k_2}\Big[2\pi i - \mathrm{Ei}(-2ik_1a) + \mathrm{Ei}(-2ik_2a) + \mathrm{Ei}(2ik_-a) \\ &+ \mathrm{Ei}(-2ik_1r) - \mathrm{Ei}(-2ik_2r) - \mathrm{Ei}(-2ik_-r) + \ln\left(\frac{r}{a}\right)\Big].\end{aligned} \tag{3.44}$$

where Ei represents the exponential integral function, which is defined as $\mathrm{Ei}(x) = -\int_{-x}^{\infty}(e^{-t}/t)dt$[38].

To facilitate our analysis of the scattering form function, we can write it as the sum of each interaction contribution as follows

$$f = f^{(\mathrm{II})} + f^{(\mathrm{IS})} + f^{(\mathrm{SI})} + f^{(\mathrm{SS})}, \tag{3.45}$$

where the super-indexes stand for the type of interaction.

3.6 Series Truncation

To compute Eq. 3.34, we have to estimate *a priori* the number of L_- of the series. Besides the same procedure should be done for the number of terms L_1 and L_2 related to the l_1 and indexes in Eq. 3.35. In doing so, we have to analyze the contribution of each interaction term in Eq. 3.35. We employ the following rule (37,38)

$$L_n \sim k_n r + c(k_n r)^{1/3}, \quad n = 1, 2, -, \tag{3.46}$$

where c is a positive constant related to the desired accuracy of the truncation; it may also depend on $k_n r$. The truncation criterion for the series in Eq. 3.35 that involve the scattering coefficient $s_{n,l}$ may be formulated based on the rule

$$\left| \frac{s_{n,0}}{s_{n,l_n+L_n}} \right| \ll 1, \quad n = 1, 2, \tag{3.47}$$

where $l_n = 0, 1, 2, ...$ Note that for the scattering-with-scattering interaction term we have, according to Eq. 3.37, that $L_- = L_1 + L_2$.

3.7 Rayleigh limit

The Rayleigh limit is valid only for the sphere size factor, where $ka < 1$. The approximate upper limit of the radius of the scatterer is generally taken to be $a = 0.05\lambda$, where λ is the wavenumber length[39]. Here, the Rayleigh limit is taken for the following conditions $k_1 a, k_2 a < 1$, which necessary implies that $k_- a < 1$. In analogy to Eqs. 3.30 and 3.31 we have

$$s^0_{n,0} = -i\frac{(k_n a)^3}{3} a^0_{n,0}, \tag{3.48}$$

$$s^m_{n,1} = -i\frac{(k_n a)^3}{6} a^m_{n,1}, \quad m = -1, 0, 1, \quad n = 1, 2. \tag{3.49}$$

According to the selection of rules in Eq. 3.37, the maximum multipole order of the form function in Eq. 3.34 is $l = 2$. Higher order moments are not allowed. That is the reason we have calculated our integrals 3.39–3.42 up to $l = 2$ and, consequently, $l_1 = l_2 = 0, 1$. On the other hand, unlike Rayleigh scattering, which has only the monopole and dipole moments, the nonlinear effect gives rise to the quadrupole moment in the scattered pressure.

3.8 Vibro-Acoustography

In medical sciences, the possibility of imaging internal structures as organ boundaries and biological tissues, is a very powerful method to identify pathologies, presence of foreign bodies, malfuctioning organs, etc.

Among the diagnosis forms, palpation is a useful technique used for centuries and is traditional example of how to estimate mechanically biological tissues abnormalities. On the other hand, if such pathology is far below to the surface or if is too small in a way that can not be detect, the palpation modality is flawed. The use of ultrasound waves to visualize internal structures represents more than 25%[40] comparing with others imaging techniques, due the fact to be a noninvasive and relatively inexpensive imaging modality. The ultrasound modality can be divided into three main categories depending upon the type of radiation considered for observe the region-of-interest: pulse-echo and harmonic imaging[41], and elastography[42]. Pulse-echo techniques are based on the linear theory of wave propagation; while harmonic imaging and some elastography methods rely on nonlinear acoustics. In particular, vibro-acoustography[17] is included in the elastography method group which was stablished as based on dynamic radiation force of ultrasound[19].

In VA system, two ultrasound beams produced by a two-element transducer at slightly different frequencies ω_1 and ω_2 are co-focused in a small volume within the region-of-interest of a sample (biological tissue or substance). As a result of nonlinear interaction of the ultrasound waves, a subharmonic component at the beat-frequency[43] $\omega_- = \omega_2 - \omega_1$ arises in the focal region. From this interaction, two acoustic waves are responsible to the VA signal. One is due to the radiation force phenomena which vibrates the sample generating a low-frequency acoustic emission

at ω_-. And the other wave is caused by the scattering of sound by sound in the focal region contributing to a scattered difference frequency generation.

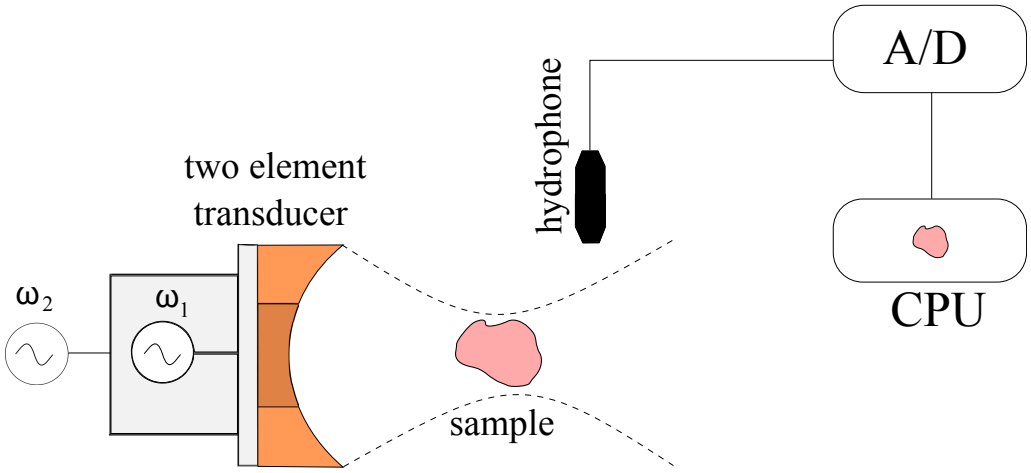

Figure 3.6: Vibro-acoustography system

A two-element confocal transducer produces a dual-frequency ultrasound beam used for illuminating the region-of-interest of a sample, Fig. 3.6. An acoustic detector is used to acquired the low-frequency acoustic field. The received signal is digitized through an analog-to-digital converter for further processing, storage and display. Moving the ultrasound beam across the sample, one can register a pixel at each discrete position in the system focal plane.

The theoretical principles of VA have been devised in terms of the dynamic radiation force produced by an amplitude-modulated ultrasound beams[17,44]. The dynamic radiation force produced upon the object in the medium[19,20] is responsible for the difference-frequency wave, which is used to form an image of the medium.

Based on the radiation force model, we may assume that the sphere emits the DF wave as a dipole. To compute the acoustic emission field, we need the amplitude of the dynamic force generated on the sphere. The force on the sphere produced by

a dual-frequency plane wave is given by[19] $\hat{f}_- = \pi a^2 E_0 \hat{Y}_-$, where $\hat{Y}_-$ is the radiation force function and $E_0 = p_0^2/\rho_0 c_0^2$, the incident energy density averaged in time. The acoustic emission (dipole) in the farfield is[45]

$$\hat{p}_{ae} = \frac{\hat{v}_c \rho_0 c_0 k_-^2 a^3 e^{ik_- a}}{2ik_- a + (k_- a)^2 - 2} \cos\theta \frac{e^{ik_- r}}{r}, \tag{3.50}$$

where $\hat{v}_c$ is the velocity amplitude of the sphere center, a is the diameter of the sphere. This velocity can be gives in terms of the dynamic radiation force as $\hat{v} = \hat{f}_-/Z_-$, where $Z_- = i(4\pi/3)a^3\omega_-\rho_1$ (ρ_1 is the density of the sphere) is the mechanical impedance of the sphere with $k_- a \ll 1$[46]. Thus, substituting $\hat{v}_c$ with the radiation force $\hat{f}_-$ into Eq. 3.50 turns to

$$|p_{ae}| = \frac{3E_0\rho_0 k_- a^2}{8\rho_1} \frac{|\cos\theta|}{r}, \tag{3.51}$$

This equation is in agreement with the acoustic field emitted by the object in the VA model[17], which yields the linear variation of the pressure with the difference-frequency. The obtained result in Eq. 3.51 will be compared with the relation to the scattered field in Eq. 3.33 in the same conditions to assess the contribution of each phenomenon to VA.

Chapter 4

RESULTS

We consider that the acoustic beams are plane waves interacting in a spherical region of radius R centered at the scatterer. It is also assumed that $R \ll r$, where r is the radial distance to the scattered. The partial wave expansion of the plane wave propagating at an arbitrary direction is given by[47]

$$\hat{p}_{I,n} = 4\pi \sum_{l,m} i^l Y_l^{m*}(\theta^*, \phi^*)(\alpha_n, \beta_n) j_l(k_n r) Y_l^m(\theta, \phi), \quad n = 1, 2, \tag{4.1}$$

where the wavevector is represented in the spherical coordinates as $\mathbf{k}_n = (k_n, \alpha_n, \beta_n)$, with α_n and β_n being the polar and azimutal angles, respectively. Comparing Eqs. 4.1 and 3.12 we find that the beam-shape coefficients are given by

$$a_{nl}^m = 4\pi i^l Y_l^{m*}(\alpha_n, \beta_n). \tag{4.2}$$

Because the region of interest to represent the plane waves is a sphere with a radius R, the partial wave expansion of each wave Eq. 4.1 should be truncated at $l = k_1 R$ and $l = k_2 R$. The factors $k_1 R$ and $k_2 R$ are the partial wave expansion bandwidth.

To evaluate the scattering form function in Eq. 3.34, we have to compute the integrals in Eq. 3.39–3.42 symbolically for $l = 0, 1, 2$ and $l_1, l_2 = 0, 1$ and for all kind

of interactions, with the aid *Mathematica* software[37]. The propagating medium under consideration is water for which $c_0 = 1500\,\mathrm{m/s}$, $\rho_0 = 1000\,\mathrm{kg/m^3}$ and $\beta = 3.5$ (at room temperature). The primary frequencies are given by $\omega_1 = \omega_0 - \omega_-/2$ and $\omega_2 = \omega_0 + \omega_-/2$. Unless specified, the center and difference-frequencies considered here are $\omega_0/2\pi = 1.5$MHz and $\omega_-/2\pi = 50$kHz, respectively. We assume also that the interacting region has radius $R = 4\pi/k_0 = 2$mm, where k_0 is the wavenumber corresponding to the center-frequency. Outside this region the primary incident waves are completely attenuated. Thus, the partial wave in Eq. 4.1 for each wave can be truncated at $l \sim k_0 R \sim 13$. Moreover, the integrals involving functions of incident waves in Eq. 3.39–3.42 should be evaluated with $r = R$.

4.1 Crossing Plane Waves

Here, we analyze the directive pattern of the scattering form function for different arrangements for intersecting plane wave. In Fig. 4.1, we exhibit the directive pattern of $|f|$, $|f^{(\mathrm{II})}|$ and $|f^{(\mathrm{SS})}|$ with the intersecting angle $\alpha_2 = 0^0$. The functions are evaluated at xz-plane with $r = 0.1\,\mathrm{m}$. The evaluation parameters are $\omega_0/2\pi = 1.5\,\mathrm{MHz}$, $\omega_-/2\pi = 50\,\mathrm{kHz}$, $R = 2\,\mathrm{mm}$, and $a = 125\,\mu\mathrm{m}$ which were the same for the directive pattern graphics (Figs. 4.1, 4.2, 4.3, 4.4) . When $\alpha_2 = 0^0$ (the beams are collinear), the scattering function has contribution from $f^{(\mathrm{II})}$ in the range $|\theta| < 90^0$. On the other hand, in the region $|\theta| > 90^0$ the scattering function has contribution from $|f^{(\mathrm{II})}|$ and $|f^{(\mathrm{SS})}|$. In this configuration the size of the interaction region R plays a major role in the difference-frequency generation.

When the intersecting angle is 45^0, which can be seen in Fig. 4.2, the scat-

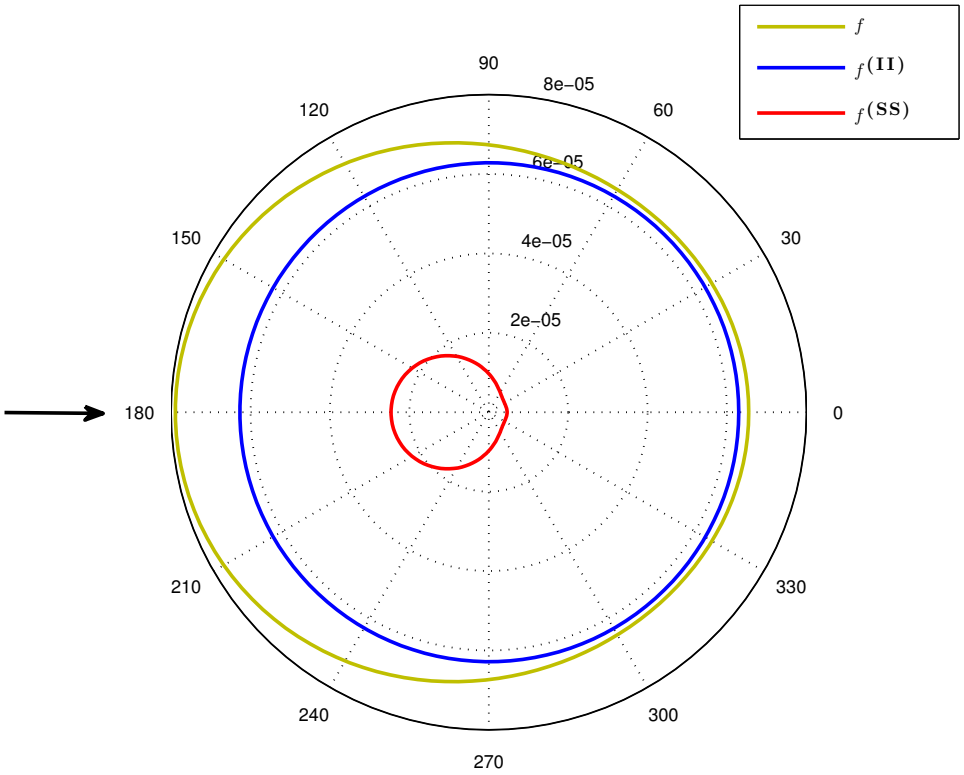

Figure 4.1: Directive pattern of the scattering form functions at the xz-plane for a intersecting angle $\alpha_2 = 0^0$. Legend: (yellow line) $|f|$, (blue line) $|f^{(\mathrm{II})}|$, and (red line) $|f^{(\mathrm{SS})}|$. The arrow indicates that the propagation of both incident waves are in the same direction.

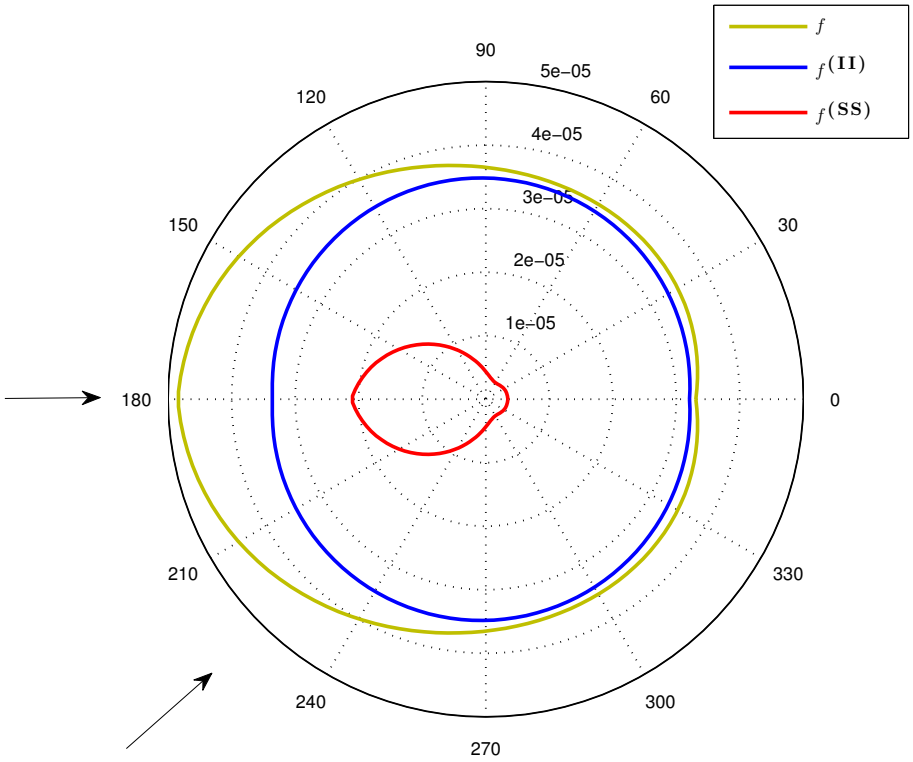

Figure 4.2: Directive pattern of the scattering form functions at the xz-plane for a intersecting angle $\alpha_2 = 45^0$. Legend: (yellow line) $|f|$, (blue line) $|f(\mathrm{II})|$, and (red line) $|f^{(\mathrm{SS})}|$. The arrows indicate the propagation direction of each incident wave.

tering function follows the same contribution for $\alpha_2 = 0^0$ with a more prominently contribution for $|\theta| < 90^0$. The scattering-with-scattering contribution is relevant in the backscattering direction. Note that for $\alpha_2 = 0^0$ and $\alpha_2 = 45^0$, the contribution of the $|f^{(\mathrm{SI})}|$ and $|f^{(\mathrm{IS})}|$ components are negligible .

For $\alpha_2 = 90^0$, Fig. 4.3, the influence of the scattering-with-scattering term is more relevant when $|\theta| > 90^0$. The incident-with-incident term is a negligible in the 90^0-configuration. This result is known from the scattering of sound-by-sound

theory[?] .

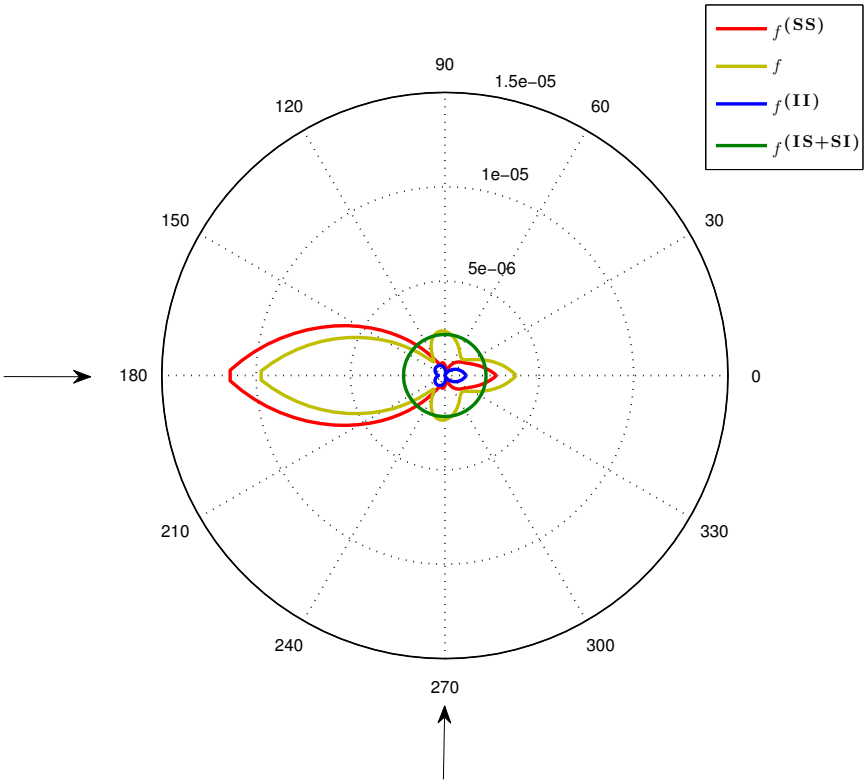

Figure 4.3: Directive pattern of the scattering form functions at the xz-plane for a intersecting angle $\alpha_2 = 90^0$. Legend: (yellow line) $|f|$, (blue line) $|f^{(\mathrm{II})}|$, (green line) $|f^{(\mathrm{IS})} + f^{(\mathrm{SI})}|$, and (red line) $|f^{(\mathrm{SS})}|$. The arrows indicate the propagation direction of each incident wave.

For the counter-propagating wave $\alpha_2 = 180^0$, which is shown in Fig. 4.4, the contributions to the scattering form function has almost the same distribution for both forward and backward distribution. For the $|f^{(\mathrm{SS})}|$ component, one can see that the distribution follows the backscattering pattern with the biggest lobe for major incident wave frequency. For the $|f^{(\mathrm{II})}|$ and $|f^{(\mathrm{IS})} + f^{(\mathrm{SI})}|$ components, the scattering pattern of both distributions are superimposed having almost the same magnitude.

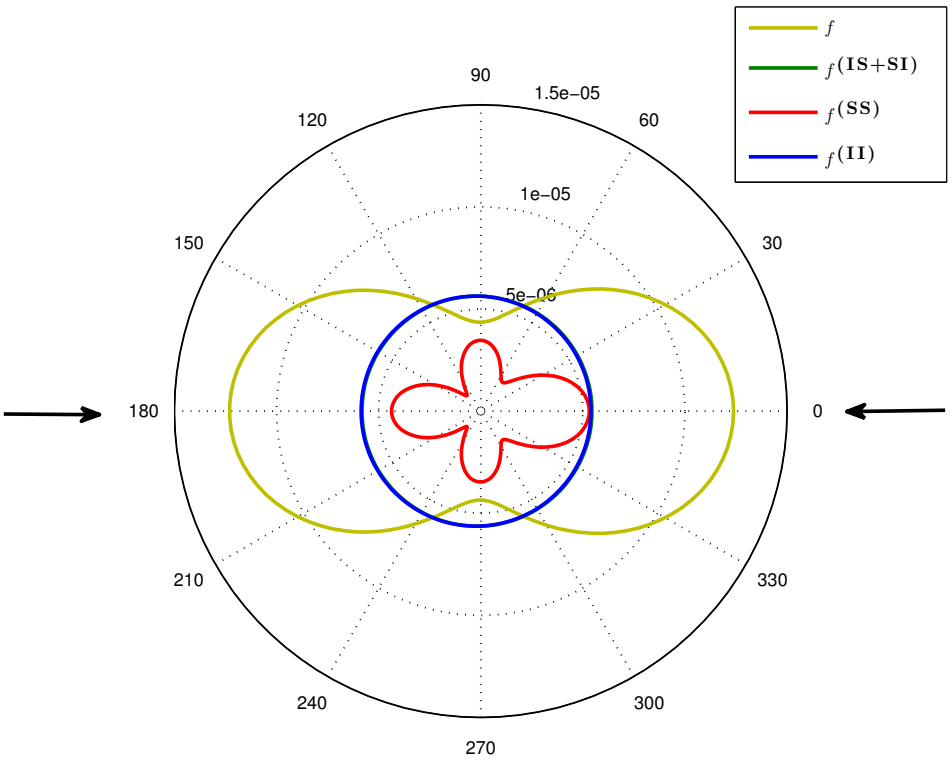

Figure 4.4: Directive pattern of the scattering form functions at the xz-plane for a intersecting angle $\alpha_2 = 180^0$. Legend: (yellow line) $|f|$, (blue line) $|f^{(\mathrm{II})}|$, (green line) $|f^{(\mathrm{IS})} + f^{(\mathrm{SI})}|$, and (red line) $|f^{(\mathrm{SS})}|$. The arrows indicate the propagation direction of each incident wave.

Chapter 5

CONCLUSIONS

The difference-frequency generation in the scattering of the two interacting acoustic waves in the Rayleigh limit by a rigid sphere was theoretically analyzed. The difference-frequency scattered pressure as the farfield was obtained as a multipole expansion series. Each moment is a result of the nonlinear interaction of all moments present in the primary (linear) scattering problem. Hence, the scattering function has contribution from all interacting partial waves involved in the scattering process. The partial wave amplitudes were given in terms of the beam-shape $a_{n,l}^{m}$ and the scattering $s_{n,l}^{m}$ coefficients. There was four possible contributions to the nonlinear interaction: incident-with-incident, incident-with-scattered, scattered-with-incident and scattered-with-scattered. The rules with determine in what manner the primary partial waves interact are imposed by Clebsch-Gordan coefficients.

The developed theoretical framework was applied to the scattering of two localized plane wave within a spherical region. The waves intersected each order at arbitrary angles. The analysis was limited to an interaction spherical region with radius R such that $R \ll r$. We numerically verified that when $R/r \sim 0.01$, the con-

tribution of the incident-with-incident term is much smaller than those from other interacting terms. Thus, the incident-with-incident term was neglected in the analysis performed here. The directive patterns of the difference-frequency scattering form function $|f(r, \theta, \varphi)|$ were plotted for plane waves having intersecting angles $\alpha_2 = 0^0, 45^0, 90^0, 180^0$. Yet the incident-with-incident and scattered-with-incident confined in a small spherical region, the jointly contribution of these terms to the scattering function is comparable to that from the scattered-with-scattered interaction. The influence of the interaction terms to scattering function may vary with the observation point. Despite this fact, the contribution of the scattered-with-scattered term is more outstanding.

The forward scattering of two collinear plane wave was analyzed varying the following parameters: radial distance, difference- and center-frequency. In all three cases, the scattering function monotonically increases as the corresponding parameter increases. Furthermore, the scattering function had more contribution from the scattered-with-scattered interaction. This fact was already been reported [25]. Assuming that this interaction is dominant, we showed that the scattered pressure varies, in the limit $(r \to \infty)$, like $r^{-1} \ln r$ with the radial distance, $\omega_- \ln \omega_-$ with the difference-frequency, and quadratically with each primary frequency. Unfortunately, there is no previous theoretical results that we can compare the present analysis with. However, the results to the pressure field found in a vibro-acoustography setup show that our difference-frequency generation based on the scattering theory are in consonance with this experimental framework. In addition to, further experiments for nonlinear scattering can be performed using instrumentation of other underwater acoustics and biomedical ultrasound instrumentation.

In conclusion, we believe that the theoretical analysis presented here is a step toward a better understanding of nonlinear scattering in acoustics. Particularly, the obtained results may be useful for acoustical imaging methods based on difference-frequency generation.

Appendix A

SURFACE INTEGRAL

According to Eq. (18) the surface integral in Eq. (20) is given by

$$I_S = -\frac{(k_- a)^2}{2k_1 k_2} \int_{4\pi} G(r, \Omega | a, \Omega') \left. \frac{\partial \mathcal{P}}{\partial r'} \right|_{r'=a} d\Omega'. \tag{A.1}$$

where $\Omega = (\theta, \phi)$. The integral will be estimated for two interacting spherical waves. Thus, the source term $\mathcal{P}$ is given by

$$\mathcal{P}(r') = \frac{e^{ik_- r'}}{k_1 k_2 r'^2}. \tag{A.2}$$

From Eq.(24) the Green's function becomes

$$G = k_- a \frac{e^{ik_- r}}{r} \sum_{l,m} \frac{(-i)^l}{h^{(1')}(k_- a)} Y_l^m(\Omega') Y_l^m(\Omega). \tag{A.3}$$

Substituting Eqs. A.2 and A.3 into Eq. A.1, yields

$$I_S = \frac{k_-^3}{2k_1^2 k_2^2} (2i + k_- a) \frac{e^{ik_-(r-a)}}{r}. \tag{A.4}$$

Appendix B

OUTER VOLUME INTEGRAL

The outer volume integral reads

$$I_\infty = \beta k_-^2 \int_r^\infty \int_{4\pi} G_\infty(r, \Omega | r', \Omega') \mathcal{P}(r', \Omega') r'^2 d\Omega', \tag{B.1}$$

where the Greens function is given by[48]

$$G = ik_- \sum_{l,m} \chi_l(k_- r) h_l^{(1)}(k_- r') Y_l^{m*}(\Omega') Y_l^m(\Omega), \quad a \leq r < r'. \tag{B.2}$$

where

$$\chi_l(k_- r) = j_l(k_- r) - \frac{j_l'(k_- a)}{h_l'^{(1)}(k_- a)} h_l'^{(1)}(k_- r) \tag{B.3}$$

We assume that the source term is due the interaction of two spherical waves as given in Eq. A.2. By substituting Eqs. A.2 and B.2 into B.1, one finds

$$I_\infty = \frac{\beta k_-}{k_1 k_2} \chi_0(k_- r) \int_r^\infty \frac{e^{2ik_- r'}}{r'} dr' \tag{B.4}$$

After integrating by parts, we obtain

$$I_\infty = \frac{\beta k_-}{k_1 k_2} \chi_0(k_- r) \left[\frac{e^{2ik_- r}}{r} + O(r^{-2}) \right]. \tag{B.5}$$

Therefore, evaluating $\chi_0(k_- r)$ through the expression of the spherical functions, we find $I_\infty = O(r^{-2})$.

Appendix C

ARTICLE

Article published on Ultrasonics

Ultrasonics 53 (2013) 470–478

Contents lists available at SciVerse ScienceDirect

Ultrasonics

journal homepage: www.elsevier.com/locate/ultras

Difference-frequency generation in nonlinear scattering of acoustic waves by a rigid sphere

Glauber T. Silva *, Anderson Bandeira

Physical Acoustics Group, Instituto de Física, Universidade Federal de Alagoas, Maceió, AL 57072-970, Brazil

ARTICLE INFO

Article history:
Received 26 June 2012
Received in revised form 24 August 2012
Accepted 25 August 2012
Available online 3 September 2012

Keywords:
Difference-frequency generation
Scattering of sound-by-sound
Partial-wave expansion

ABSTRACT

In this paper, the partial-wave expansion method is applied to describe the difference-frequency pressure generated in a nonlinear scattering of two acoustic waves with an arbitrary wavefront by means of a rigid sphere. Particularly, the difference-frequency generation is analyzed in the nonlinear scattering with a spherical scatterer involving two intersecting plane waves in the following configurations: collinear, crossing at right angles, and counter-propagating. For the sake of simplicity, the plane waves are assumed to be spatially located in a spherical region which diameter is smaller than the difference-frequency wavelength. Such arrangements can be experimentally accomplished in vibro-acoustography and nonlinear acoustic tomography techniques. It turns out to be that when the sphere radius is of the order of the primary wavelengths, and the downshift ratio (i.e. the ratio between the fundamental frequency and the difference-frequency) is larger than five, difference-frequency generation is mostly due to a nonlinear interaction between the primary scattered waves. The exception to this is the collinear scattering for which the nonlinear interaction of the primary incident waves is also relevant. In addition, the difference-frequency scattered pressure in all scattering configurations decays as $r^{-1}\ln r$ and $1/r$, where r is the radial distance from the scatterer to the observation point.

1. Introduction

An outstanding feature of the nonlinear interaction of two or more acoustic waves is a generation of secondary waves having different frequencies, namely harmonics, sum- and difference-frequency [1]. In the presence of an inclusion, this generation is enhanced by two physical effects. First of all, the incident waves produce a radiation force through nonlinear interactions with the inclusion [2–5]. As a result, the inclusion is set in motion emitting waves which frequencies correspond to the components present in the dynamic radiation force. In addition, the primary waves (incident and scattered) related to the fundamental frequencies interact yielding secondary waves. This process is also known as scattering of sound-by-sound in which sum- and difference-frequency waves are generated [6–9].

Difference-frequency generation is present in several applications like parametric array sonar [10], audio spotlight [11], characterization of liquid–vapor phase-transition [12], and acoustical imaging methods such as nonlinear parameter tomography [13–16] and vibro-acoustography [17–19]. Moreover, parametric arrays have been used to produce low-frequency waves in wideband scattering experiments [20]. In this case, the scatterer is placed outside the interaction region of the incident waves and the scattering is treated through the linear scattering theory. This is similar to calibrating parametric sonars based on measurements of the linear scattering cross-section [21].

Investigations of difference- and sum-frequency generation concerning to spherical and cylindrical scattered waves were firstly performed by Dean [22]. Scattering consisting of nonlinear interaction of a plane wave with a radially vibrating rigid cylinder [23] and sphere [24] have also been analyzed. Moreover, difference-frequency generation in scattering of two collinear plane waves by means of a sphere was previously studied [25]. However, the results obtained in this study show that the difference-frequency scattered pressure has singularities in the polar angle of spherical coordinates (i.e. the angle formed by the position vector and the z-axis). Furthermore, the difference-frequency scattered pressure only depends on the monopole terms of the primary waves. Giving this physical picture, a broader discussion is required on how to handle the singularities and why the information from higher-order multipole terms of the primary waves were discarded.

Applications of difference-frequency generation in acoustics generally employ incident beams which deviate from collinear plane waves. This has stimulated the investigation of nonlinear scattering of two acoustic waves with an arbitrary wavefront.

* Corresponding author.
E-mail address: glauber@pq.cnpq.br (G.T. Silva).

0041-624X/$ - see front matter © 2012 Elsevier B.V. All rights reserved.
http://dx.doi.org/10.1016/j.ultras.2012.08.015

Our analysis stems from the Westervelt wave equation [26]. This equation is solved through the method of successive approximations in addition to the Green's function technique. Furthermore, appropriate boundary conditions are established to guarantee a unique solution of the Westervelt equation. The difference-frequency scattered pressure is obtained as a partial-wave expansion which depends on beam-shape and scattering coefficients. Each of these coefficients is related, respectively, to a complex amplitude of a partial-wave that composes the primary incident and scattered waves [27,28].

The method proposed here is applied to the nonlinear scattering of two intersecting plane waves by a rigid sphere. The difference-frequency scattered pressure is obtained in the farfield in three incident wave configurations: collinear, perpendicular, and counter-propagating. In this analysis, the downshift ratio is larger than five. It is worthy to mention that the collinear configuration of incident waves has been implemented in vibro-acoustography experiments [17], while the perpendicular and counter-propagating arrangements have been experimentally studied in Refs. [14,15], respectively. To reduce the mathematical complexity of the model, the incident waves are assumed to be spatially located in a spherical region. Even though this approach is not entirely realistic, experimental accomplishment of scattering of two located intersecting ultrasound beams was reported in Ref. [29].

The results show that in the collinear case, the nonlinear interaction involving the primary incident waves (incident-with-incident interaction) and that of the primary scattered waves (scattered-with-scattered interaction) are responsible for difference-frequency generation. In the perpendicular and counter-propagating configurations, difference-frequency generation is mostly due to the scattered-with-scattered interaction. In addition, the difference-frequency scattered pressure increases with difference-frequency and varies with the radial distance r from the scatterer to observation point as $r^{-1}\ln r$ and $1/r$. A similar result is found in Ref. [22], though only monopole sources were considered.

2. Physical model

Consider a nonviscous fluid with an ambient density ρ_0 and an adiabatic speed of sound c_0. The fluid is assumed to have infinite extent. Acoustic waves in the fluid can be described by the acoustic pressure p as a function of the position vector $\mathbf{r}$ and time t. Absorption effects of a viscous fluid can be readily included for longitudinal acoustic waves (compressional waves). In this case, the wavenumber of a single-frequency wave becomes a complex number. However, the account for shear wave propagation, which is supported in viscous fluids, lies beyond the scope of this study.

2.1. Wave dynamics

We are interested on describing how a difference-frequency wave is generated in a nonlinear scattering of two incident acoustic waves by means of a rigid sphere. The scope of this analysis is limited to acoustic pressures propagating in the farfield. Up to second-order approximation, the farfield pressure satisfies the lossless Westervelt wave equation [30]

$$\left(\nabla^2-\frac{1}{c_0^2}\frac{\partial^2}{\partial t^2}\right)p=-\frac{\beta}{\rho_0 c_0^4}\frac{\partial^2 p^2}{\partial t^2}, \tag{1}$$

where $\beta=1+(1/2)(B/A)$, with B/A being the thermodynamic nonlinear parameter of the fluid. This equation accounts for wave diffraction and medium nonlinearity. It is worthy to notice that Eq. (1) is valid when cumulative effects (such as wave distortion) are dominant over nonlinear local effects. This happens when the propagating wave is far from acoustic sources. When the wave is observed near to a scatterer, its pressure should be modified to [31]

$$\tilde{p}=p+\frac{\rho_0}{4}\left(\nabla^2+\frac{1}{c_0^2}\frac{\partial^2}{\partial t^2}\right)\phi^2. \tag{2}$$

where ϕ is the velocity potential. Note that the approximation $\tilde{p}=p$ holds for farfield waves.

Let us assume that the acoustic pressure is given in terms of the Mach number $\varepsilon=v_0/c_0$ and $\varepsilon\ll 1$ (weak-amplitude waves), where v_0 is the maximum magnitude of the particle velocity in the medium. Hence, we can expand the pressure up to second-order as [32]

$$p=\varepsilon p^{(1)}+\varepsilon^2 p^{(2)},\quad \varepsilon\ll 1, \tag{3}$$

where $p^{(1)}$, and $p^{(2)}$ are, respectively, the linear (primary) and the second-order (secondary) pressure fields. In the weak-amplitude approximation ($\varepsilon\ll 1$), the primary and the secondary pressures suffice to describe nonlinear effects in wave propagation. Now, substituting Eq. (3) into Eq. (1) and grouping terms of like powers ε and ε^2, one obtains

$$\left(\nabla^2-\frac{1}{c_0^2}\frac{\partial^2}{\partial t^2}\right)p^{(1)}=0, \tag{4}$$

$$\left(\nabla^2-\frac{1}{c_0^2}\frac{\partial^2}{\partial t^2}\right)p^{(2)}=-\frac{\beta}{\rho_0 c_0^4}\frac{\partial^2 p^{(1)2}}{\partial t^2}. \tag{5}$$

These equations form a set of hierarchical linear wave equations.

2.2. Linear scattering

Assume that two primary acoustic waves of arbitrary wavefront with frequencies ω_1 and ω_2 ($\omega_2>\omega_1$), propagate toward a scatterer suspended in a host fluid. The total incident pressure due to the waves is given by

$$p_i=\varepsilon\rho_0 c_0^2(\hat{p}_{i,1}e^{-i\omega_1 t}+\hat{p}_{i,2}e^{-i\omega_2 t}), \tag{6}$$

where i is the imaginary unit, $\hat{p}_{i,1}$ and $\hat{p}_{i,2}$ are the dimensionless pressure amplitudes of the incident waves. When the scatterer is placed in the interaction region of the incident waves (see Fig. 1), two primary scattered waves appear in the medium. Hence, the primary scattered pressure reads

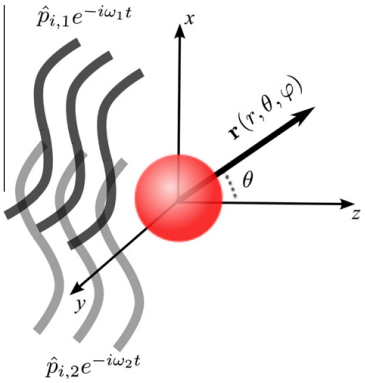

Fig. 1. Outline of the scattering problem. Two incident waves of arbitrary wavefront with amplitudes $\hat{p}_{i,1}$ and $\hat{p}_{i,2}$ insonify a target. The observation point is denoted in spherical coordinates by $\mathbf{r}(r,\theta,\varphi)$, where r is the radial distance from the scatterer to the observation point, θ and φ are the polar and the azimuthal angles, respectively.

$$p_s = \varepsilon\rho_0 c_0^2(\hat{p}_{s,1}e^{-i\omega_1 t} + \hat{p}_{s,2}e^{-i\omega_2 t}), \tag{7}$$

where $\hat{p}_{s,1}$ and $\hat{p}_{s,2}$ are the dimensionless pressure amplitudes of the scattered waves. Therefore, the total primary pressure in the fluid is then $p^{(1)} = p_i + p_s$.

It is worthy to notice that the quadratic term $\partial^2 p^{(1)2}/\partial t^2$ in Eq. (5) gives rise to waves at second-harmonic frequencies $2\omega_1$ and $2\omega_2$, sum-frequency $\omega_1 + \omega_2$, and difference-frequency $\omega_2 - \omega_1$. These frequency components are distinct and do not affect each other. Our analysis is restricted to the difference-frequency component only.

By substituting Eqs. (6) and (7) into Eq. (4), we find that the primary pressure amplitudes satisfy the Helmholtz equation

$$\left(\nabla^2 + k_n^2\right)\begin{pmatrix}\hat{p}_{i,n}\\ \hat{p}_{s,n}\end{pmatrix} = 0, \quad n = 1, 2, \tag{8}$$

where $k_n = \omega_n/c_0$ is the primary wavenumber.

The incident pressure amplitudes are assumed to be regular (finite) in the origin of the coordinate system. Thus, they are given, in spherical coordinates (radial distance r, polar angle θ, azimuthal angle φ) by [33]

$$\hat{p}_{i,n} = \sum_{l,m} a_{nl}^m j_l(k_n r) Y_l^m(\theta, \varphi), \quad n = 1, 2, \tag{9}$$

where $\sum_{lm} \to \sum_{l=0}^{\infty}\sum_{m=-l}^{l}$, a_{nl}^m is the beam-shape coefficient, j_l is the spherical Bessel function of lth-order and Y_l^m is the spherical harmonic of lth-order and mth-degree. The beam-shape coefficients can be determined by using the orthogonality property of the spherical harmonics. Numerical quadrature can be used to compute these coefficients for waves with arbitrary wavefront [27,28].

The scattered pressure amplitudes are given by [34]

$$\hat{p}_{s,n} = \sum_{l,m} s_{nl}^m h_l^{(1)}(k_n r) Y_l^m(\theta, \varphi), \quad n = 1, 2, \tag{10}$$

where $h_l^{(1)}$ is the first-type spherical Hankel function of lth-order and s_{nl}^m is the scattering coefficient to be determined from acoustic boundary conditions on the scatterer's surface.

2.3. Difference-frequency generation

The generated difference-frequency pressure is a second-order field in the Mach number expansion (3). Thus, we may express the difference-frequency pressure as

$$p_- = \varepsilon^2\rho_0 c_0^2 \hat{p}_- e^{-i\omega_- t}, \tag{11}$$

where $\hat{p}_-$ is the dimensionless difference-frequency pressure amplitude and $\omega_- = \omega_2 - \omega_1$. Substituting Eq. (11) into Eq. (5) we find that $\hat{p}_-$ satisfies the inhomogeneous Helmholtz equation

$$(\nabla^2 + k_-^2)\hat{p}_- = \beta k_-^2 \mathcal{P}, \tag{12}$$

where $k_- = \omega_-/c_0$ is the difference-frequency wavenumber and

$$\mathcal{P} = \hat{p}_{i,1}^* \hat{p}_{i,2} + \hat{p}_{i,1}^* \hat{p}_{s,2} + \hat{p}_{s,1}^* \hat{p}_{i,2} + \hat{p}_{s,1}^* \hat{p}_{s,2}, \tag{13}$$

with the symbol $*$ meaning complex conjugation. The source term $\mathcal{P}$ corresponds to all possible interactions between the primary waves which generate the difference-frequency pressure.

2.4. Boundary conditions

The uniqueness of solutions of Eqs. (8) and (12) depend on the acoustic boundary conditions across the scatterer object boundary. To find these conditions the physical constraints of the scattering problem should be analyzed.

First of all, the presence of primary and secondary pressures induces the object itself to move. Consequently, an acoustic emission by the object takes place in the host fluid, which means further scattering. If both the object density is large and its compressibility is small compared to those of the host fluid, the acoustic emission represents only a small correction to the main scattering due to the presence of the object in the medium [35]. In our analysis, this correction is neglected and the object is considered immovable. Therefore, the boundary condition for a rigid and immovable sphere of radius a is that the normal component of the particle velocity should vanish on the sphere's surface.

The particle velocity is given in second-order approximation as

$$\mathbf{v} = \varepsilon\mathbf{v}^{(1)} + \varepsilon^2\mathbf{v}^{(2)}, \quad \varepsilon \ll 1, \tag{14}$$

where $\mathbf{v}^{(1)}$ and $\mathbf{v}^{(2)}$ are the linear and the second-order velocity fields, respectively. Thus, for the linear velocity we have $\mathbf{v}^{(1)} \cdot \mathbf{e}_r|_{r=a} = 0$, where $\mathbf{e}_r$ is the outward normal unit-vector on the sphere's surface. From the linear momentum conservation equation $\rho_0(\partial\mathbf{v}^{(1)}/\partial t) = -\nabla p^{(1)}$, we find the following condition for the primary total pressure

$$\left[\frac{\partial(\hat{p}_{i,n} + \hat{p}_{s,n})}{\partial r}\right]_{r=a} = 0. \tag{15}$$

This is known as the Neumann boundary condition. After substituting Eqs. (6) and (10) into this equation, one obtains the scattering coefficient as $s_{nl}^m = s_{nl}a_{nl}^m$, where

$$s_{nl} = -\frac{j_l'(k_n a)}{h_l^{(1)\prime}(k_n a)}, \tag{16}$$

with the prime symbol meaning derivation.

The second-order particle velocity satisfies the conservation equation [36]

$$\rho_0\frac{\partial\mathbf{v}^{(2)}}{\partial t} + \nabla(p^{(2)} + \mathcal{L}) = 0, \tag{17}$$

where $\mathcal{L} = (\rho_0/4)\Box^2\phi^{(1)2}$ is the Lagrangian density of the wave, with $\Box^2$ being the d'Alembertian operator. The function $\phi^{(1)}$ is the first-order velocity potential. Projecting Eq. (17) on $\mathbf{e}_r$ at the sphere's surface, one finds

$$\left.\frac{\partial p^{(2)}}{\partial r}\right|_{r=a} = -\left.\frac{\partial\mathcal{L}}{\partial r}\right|_{r=a}. \tag{18}$$

Now, using the linear relation $p^{(1)} = \rho_0(\partial\phi^{(1)}/\partial t)$, Eqs. (2) and (18), one obtains the boundary condition for the difference-frequency pressure as

$$\left.\frac{\partial\hat{p}_-}{\partial r}\right|_{r=a} = -\frac{k_-^2}{2k_1k_2}\left.\frac{\partial\mathcal{P}}{\partial r}\right|_{r=a}. \tag{19}$$

2.5. Green's function approach

The solution of Eq. (12) can be obtained through the Green's function method. Because the normal derivative of the difference-frequency pressure is specified on the sphere's surface, the normal derivative of the Green's function on this surface should vanish in order to avoid overspecification in the method. Thereby, the difference-frequency pressure amplitude is given in terms of the Green's function $G(\mathbf{r}|\mathbf{r}')$ by [37]

$$\hat{p}_-(\mathbf{r}) = -\beta k_-^2\int_V \mathcal{P}(\mathbf{r}')G(\mathbf{r}|\mathbf{r}')dV' + \frac{(\nabla^2 - k_-^2)\mathcal{P}}{4k_1k_2} - \frac{k_-^2}{2k_1k_2} \times \int_S\left(\frac{\partial\mathcal{P}}{\partial\mathbf{r}'}\right)_{r'=a} G(\mathbf{r}|\mathbf{r}')dS', \tag{20}$$

where S denotes the sphere's surface and V is the volume of the spatial region from S to infinity. Note that Eqs. (2) and (19) have been

used in the derivation of Eq. (20). The second term in the right-hand side of Eq. (20) is related to the second term in the right-hand side of Eq. (2).

The contribution of the surface integral for two interacting spherical waves (monopoles) is found to be $k_-^3/(k_1k_2)^2$ in Appendix A. In contrast, it will be shown in Eq. (25) that the magnitude of the volume integral in Eq. (20) is proportional to $\beta k_-/(k_1k_2)$. Thus, the ratio of the volume to the surface integral is $k_-^2/(\beta k_1k_2)$. It is convenient to write the primary angular frequencies in a symmetric way as follows $\omega_1=\omega_0-\omega_-/2$ and $\omega_2=\omega_0+\omega_-/2$, where ω_0 is the mean frequency. Now the ratio between the integrals can be expressed as $\beta^{-1}[(\omega_0/\omega_-)^2-1/4]^{-1}$. Note that ω_0/ω_- is the downshift ratio. If the contribution from the surface integral is about 0.01 of that from the volume integral in water, the downshift ratio should be larger than five. Therefore, limiting our analysis to downshift ratios larger than five, we can neglect the surface integral in Eq. (20).

The volume integral in Eq. (20) can be split into two regions: $a\leqslant r'<r$ (inner source volume) and $r<r'$ (outer source volume). In Appendix B, the integral corresponding to the outer volume is estimated for two interacting spherical waves. The result shows that this integral is $O(r^{-2})$. It will be demonstrated that the inner volume integral evaluated in the farfield $k_-r\gg 1$ is $O(r^{-1})$. Hence, keeping only $O(r^{-1})$ terms in the difference-frequency scattered pressure, the contribution of the outer volume integral can be neglected.

The contribution of the second term in the right-hand side of Eq. (20), i.e. the term related to local effects, in the farfield is $O(r^{-2})$ as long as the incident waves behave as $O(r^{-1})$ in the farfield. Therefore, in the farfield the difference-frequency pressure amplitude is given by

$$\hat{p}_-(\mathbf{r})\simeq-\beta k_-^2\int_a^r\int_\Omega \mathcal{P}(\mathbf{r}')G(\mathbf{r}|\mathbf{r}')r'^2\,dr'\,d\Omega', \tag{21}$$

where $d\Omega'$ is the infinitesimal solid angle and the integration is performed on the surface of the unit-sphere Ω.

In the region $r'<r$, the Green's function which satisfies the Neumann boundary condition on the sphere's surface is given by [38]

$$G=ik_-\sum_{l,m}h_l^{(1)}(k_-r)\chi_l(k_-r')Y_l^m(\theta,\varphi)Y_l^{m*}(\theta',\varphi'), \tag{22}$$

where

$$\chi_l(k_-r')=j_l(k_-r')-\frac{j_l'(k_-a)}{h_l^{(1)'}(k_-a)}h_l^{(1)}(k_-r'). \tag{23}$$

After using the large argument approximation of the spherical Hankel function [40] in Eq. (22), we find the Green's function in the farfield as

$$G=\frac{e^{ik_-r}}{r}\sum_{l,m}i^{-l}\chi_l(k_-r')Y_l^m(\theta,\varphi)Y_l^{m*}(\theta',\varphi'). \tag{24}$$

Now, substituting this equation into Eq. (21) along with Eqs. (6) and (10), we obtain the difference-frequency scattered pressure amplitude in the farfield as

$$\hat{p}_-(r,\theta,\varphi)=\frac{\beta k_-}{k_1k_2}f_-(r,\theta,\varphi)\frac{e^{ik_-r}}{r},\quad k_-r\gg 1, \tag{25}$$

where

$$f_-(r,\theta,\varphi)=\sum_{l,m}S_l^m(r)Y_l^m(\theta,\varphi) \tag{26}$$

is the difference-frequency scattering form function. The interaction function is expressed as

$$S_l^m=-i^{-l}\sum_{l_1,m_1}\sum_{l_2,m_2}\sqrt{\frac{(2l_1+1)(2l_2+1)}{4\pi(2l+1)}}\times C_{l_1,0,l_2,0}^{l,0}C_{l_1,m_1,l_2,m_2}^{l,m}a_{1,l_1}^{m_1*}a_{2,l_2}^{m_2}\times\left(\varrho_{l_1l_2l}^{(\mathrm{II})}+s_{1,l_1}^*\varrho_{l_1l_2l}^{(\mathrm{SI})}+s_{2,l_2}\varrho_{l_1l_2l}^{(\mathrm{IS})}+s_{1,l_1}^*s_{2,l_2}\varrho_{l_1l_2l}^{(\mathrm{SS})}\right), \tag{27}$$

where $C_{l_1,m_1,l_2,m_2}^{l,m}$ is the Clebsch–Gordan coefficient, which come from the angular integration through the identity [41]

$$\int_\Omega Y_{l_1}^{m_1}Y_{l_2}^{m_2}Y_l^m\,d\Omega=(-1)^m\sqrt{\frac{(2l_1+1)(2l_2+1)}{4\pi(2l+1)}}\times C_{l_1,0,l_2,0}^{l,0}C_{l_1,m_1,l_2,m_2}^{l,-m}. \tag{28}$$

The Clebsh–Gordan coefficient satisfies the following conditions [42]

$$\begin{aligned}&m_1+m_2=m,\\&|l_2-l_1|\leqslant l\leqslant l_1+l_2,\end{aligned} \tag{29}$$

otherwise it values zero. Furthermore, when $m_1=m_2=m=0$ the l_1+l_2+l should be even, otherwise the coefficient becomes zero. The cumulative radial functions $\varrho^{(\cdot)}$ stands for each possible interaction of the primary waves, i.e. incident-with-incident (II), scattered-with-incident (SI), incident-with-scattered (IS), and scattered-with-scattered (SS). They are given by

$$\varrho_{l_1l_2l}^{(\mathrm{II})}=k_1k_2k_-\int_a^r\chi_l(k_-r')j_{l_1}(k_1r')j_{l_2}(k_2r')r'^2\,dr', \tag{30}$$

$$\varrho_{l_1l_2l}^{(\mathrm{IS})}=k_1k_2k_-\int_a^r\chi_l(k_-r')j_{l_1}(k_1r')h_{l_2}^{(1)}(k_2r')r'^2\,dr', \tag{31}$$

$$\varrho_{l_1l_2l}^{(\mathrm{SI})}=k_1k_2k_-\int_a^r\chi_l(k_-r')h_{l_1}^{(2)}(k_1r')j_{l_2}(k_2r')r'^2\,dr', \tag{32}$$

$$\varrho_{l_1l_2l}^{(\mathrm{SS})}=k_1k_2k_-\int_a^r\chi_l(k_-r')h_{l_1}^{(2)}(k_1r')h_{l_2}^{(1)}(k_2r')r'^2\,dr'. \tag{33}$$

Equations (25) and (26) along with Eqs. (30)–(33) describe the difference-frequency generation in the nonlinear scattering of two primary incident waves with arbitrary wavefront from a spherical target.

In the upcoming analysis, it is useful to decompose the difference-frequency pressure amplitude following the contribution of each primary interaction as given in Eq. (27). Accordingly, we write

$$\hat{p}_-=\hat{p}_-^{(\mathrm{II})}+\hat{p}_-^{(\mathrm{IS,SI})}+\hat{p}_-^{(\mathrm{SS})}, \tag{34}$$

where the super-indexes stand for the interaction of the primary waves and $\hat{p}^{(\mathrm{IS,SI})}=\hat{p}^{(\mathrm{IS})}+\hat{p}^{(\mathrm{SI})}$. According to Eq. (13) each term in Eq. (34) is related to the primary pressure as follows: $\hat{p}_{i,1}^*\hat{p}_{i2}\to\hat{p}_-^{(\mathrm{II})}$, $\left(\hat{p}_{i,1}^*\hat{p}_{s,2}+\hat{p}_{s,1}^*\hat{p}_{i,2}\right)\to\hat{p}_-^{(\mathrm{IS,SI})}$, and $\hat{p}_{s,1}^*\hat{p}_{s,2}\to\hat{p}_-^{(\mathrm{SS})}$.

We will show later that the scattered-with-scattered interaction provides the most relevant contribution to difference frequency generation analyzed here. Thus, let us examine the asymptotic behavior of $\varrho_{l_1l_2l}(r)^{(\mathrm{SS})}$ with $k_-r\gg 1$. In doing so, we introduce a new variable $u=r'/r$ in Eq. (33) and then

$$\varrho_{l_1l_2l}^{(\mathrm{SS})}(r)=k_1k_2k_-r^3\int_{a/r}^1\chi_l(k_-ru)h_{l_1}^{(2)}(k_1ru)h_{l_2}^{(1)}(k_2ru)u^2\,du. \tag{35}$$

Since the integrand uniformly approaches to the product of the asymptotic formulas of the spherical functions with large argument in the interval $a/r\leqslant u\leqslant 1$, then in the farfield this integral can be written as [47]

$$\varrho_{l_1l_2l}^{(\mathrm{SS})}(r)=i^{l_1-l_2}\times\int_{a/r}^1\left[\sin\left(k_-ru-\frac{l\pi}{2}\right)-\frac{i^{-l-1}j_l'(k_-a)}{h_l^{(1)'}(k_-a)}e^{ik_-ru}\right]\frac{e^{ik_-ru}}{u}\,du. \tag{36}$$

Therefore,

$$\varrho_{l_1l_2l}^{(\mathrm{SS})}(r)=-\frac{i^{l+l_1-l_2-1}}{2}\left\{\ln\left(\frac{r}{a}\right)-(-1)^l\left(\frac{2j_l'(k_-a)}{h_l^{(1)\prime}(k_-a)}-1\right)[i\pi-\mathrm{Ei}(2ik_-a)]\right\},\quad k_-r\gg 1, \tag{37}$$

where Ei is the exponential integral function.

As a result, the contribution provided by the scattered-with-scattered interaction to the difference-frequency scattered pressure varies with the radial distance r as follows

$$\hat{p}_-^{(SS)} = A_1 \frac{\ln r}{r} + \frac{A_2}{r}, \tag{38}$$

where A_1 and A_2 are constants to be determined from Eqs. (25)–(27). The $r^{-1}\ln r$ term happens only in regions containing primary energy (volume sources). Furthermore, it is known as "continuously pumped sound waves", while the $1/r$ term is called "scattered sound wave" [9].

2.6. Difference-frequency scattered power

The scattered power at difference-frequency is given by

$$P_-(r) = \frac{\varepsilon^4 \rho_0 c_0^3 r^2}{2} \int_\Omega \mathrm{Re}\{\hat{p}_-^* \hat{\mathbf{v}}_-\} \cdot \mathbf{e}_r \, d\Omega, \tag{39}$$

where 'Re' means the real-part and the amplitude $\hat{\mathbf{v}}_-$ comes from the difference-frequency particle velocity $\mathbf{v}_- = \varepsilon^2 c_0 \hat{\mathbf{v}}_- e^{-i\omega_- t}$. In the farfield, cumulative effects are dominant in difference-frequency generation. Thus, referring to Eq. (17) we find that $\hat{\mathbf{v}}_- \simeq -(i/k_-)\nabla \hat{p}_-$. After using this result along with Eq. (25) and (26) into Eq. (39), one obtains

$$P_-(r) = \frac{\varepsilon^4 \rho_0 c_0^3 \beta^2 k_-^2}{2k_1^2 k_2^2} \sum_{l,m} \left|S_l^m(r)\right|^2. \tag{40}$$

According to Eq. (38) the difference-frequency scattered pressure varies logarithmically with the radial distance r. This result is also known for two concentric outgoing spherical waves [22]. Consequently, the scattered power given in Eq. (40) will increase without limit as $r \to \infty$, unless some account is taken to absorption processes of the primary waves.

2.7. Series truncation

To compute Eq. (26), we have to estimate *a priori* the number of terms L_- in order to truncate the infinite series. This is done by performing a truncation of the incident partial-wave expansion given in Eq. (6). Let L_1 and L_2 be the truncation orders corresponding to the series expansions of the primary waves (incident or scattered) with frequency ω_1 and ω_2, respectively. The parameters L_1 and L_2 are related, respectively, to the indexes l_1 and l_2 in Eq. (27). To determined L_1 and L_2, we employ the following rule [43,44]

$$L_n \sim k_n x + c(k_n x)^{1/3}, \quad n = 1, 2, \tag{41}$$

where c is a positive constant related to the truncation numerical precision, and x is a characteristic dimension involved in the wave propagation. For instance, x can be the scatterer radius or a linear dimension of an interaction region of the incident waves. Once L_1 and L_2 are established, the truncation order L_- of Eq. (26) is given through Eq. (29) as $L_- = L_1 + L_2$.

3. Results and discussion

To illustrate the solution obtained for the difference-frequency scattered pressure given in Eq. (25), we consider a spherical scatterer suspended in water, in which $c_0 = 1500\ \mathrm{m/s}$, $\rho_0 = 1000\ \mathrm{kg/m^3}$, and $\beta = 3.5$ (at room temperature). The sphere is insonified by two intersecting plane waves which are confined in a spherical region of radius R. This region is centered on the scatterer as shown in Fig. 2. The incident wavevectors are denoted by $\mathbf{k}_1$ and $\mathbf{k}_2$. Yet this model is not entirely realistic, spatially confined plane waves with fast spatial decay can be experimentally produced by means of focused transducers [29].

The partial wave expansion of each plane wave is given by [39]

$$\hat{p}_{i,n} = 4\pi \sum_{l,m} i^l Y_l^{m*}(\theta_n, \varphi_n) j_l(k_n r) Y_l^m(\theta, \varphi), \quad r \leqslant R, \tag{42}$$

where $n = 1, 2$ and $\mathbf{k}_n$ is given in terms of $(k_n, \theta_n, \varphi_n)$, with θ_n and φ_n being the polar and azimuthal angles, respectively. Comparing Eqs. (42) and (6) we find that the beam-shape coefficient is given by

$$a_{nl}^m = 4\pi i^l Y_l^{m*}(\theta_n, \varphi_n). \tag{43}$$

For radial distances larger than R the incident pressure amplitude vanishes, i.e. $\hat{p}_{i,n} = 0$. Hence, the integration interval of Eqs. (30)–(32) should be $a \leqslant r' \leqslant R$.

The scattering problem can be further simplified by assuming that one plane wave propagates along the z-axis, thus, $\mathbf{k}_1 = k_1 \mathbf{e}_z$, with $\mathbf{e}_z$ is the Cartesian unit-vector along the z-axis. Whereas the other wave travels along the direction determined by $\mathbf{k}_2 = \sin(\theta_2)\mathbf{e}_x + k_2 \cos(\theta_2)\mathbf{e}_z$, where $\mathbf{e}_x$ is the Cartesian unit-vector along the x-axis. Unless specified, the scatterer radius is $a = 1$ mm, the spherical region of the plane waves has radius $R = 2.4$ mm, the radial observation distance is $r = 0.1$ m, and the mean- and the difference-frequency are $\omega_0/2\pi = 1.5$ MHz and $\omega_-/2\pi = 100$ kHz, respectively. Thus, the downshift ratio is fifteen. These parameters are in the same range as those used in some nonlinear acoustical imaging methods [14,15,29]. The size factors involved in the scattering problem are $k_-R = 1$, $k_1R = 14.5$, $k_2R = 15.5$, $k_-a = 0.41$, $k_1a = 6.07$, $k_2a = 6.49$, $k_-r = 41.88$, $k_1r = 607.37$, and $k_2r = 649.26$. The truncation orders are determined by setting the parameter $c = 4$ (four precision digits) in Eq. (41). Hence, the truncation orders for $\hat{p}_-^{(II)}$, $\hat{p}_-^{(IS)}$, $\hat{p}_-^{(SI)}$, and $\hat{p}_-^{(SS)}$ are respectively given by $(L_-, L_1, L_2) = (69, 33, 36), (48, 33, 15), (51, 15, 36), (29, 14, 15)$.

The integrals in Eqs. (30)–(33) can be solved analytically for arbitrary combinations of the indexes l, l_1, and l_2. Nevertheless, the number of terms in the solution grows combinatorially with the indexes. In the present example, the analytic solution of the integrals seems not to be practical. Hence, the integrals are solved numerically by using the Gauss–Kronrod quadrature method [45].

The directive pattern in the xz-plane of the difference-frequency scattered pressure given in Eq. (25) and produced by two collinear plane waves ($\theta_2 = 0$) are shown in Fig. 3. The dimensionless pressures $\hat{p}_-^{(II)}$, $\hat{p}_-^{(IS,SI)}$, and $\hat{p}_-^{(SS)}$ are also exhibited. The magnitudes of these functions are normalized to the maximum value of $|\hat{p}|$ which is 0.0807. The contribution from $\hat{p}_-^{(IS,SI)}$ is small compared to other dimensionless pressures. In the region $30^\circ < \theta < 330^\circ$, the difference-frequency scattered pressure is dominated by $\hat{p}_-^{(II)}$. Both $\hat{p}_-^{(II)}$ and $\hat{p}_-^{(SS)}$ give a prominent contribution to the difference-frequency scattered pressure when $\theta < 30^\circ$ and $\theta > 330^\circ$. In this case, the contribution of $\hat{p}_-^{(II)}$ corresponds to 25% of the scattered difference-fre-

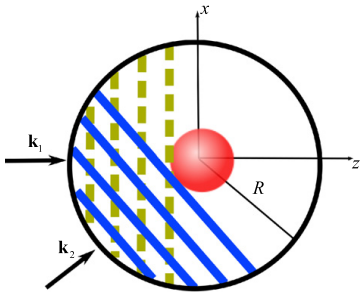

Fig. 2. Scattering of two confined plane waves from a sphere of radius a. The wavevectors are denoted by $\mathbf{k}_1$ and $\mathbf{k}_2$. The incident plane waves propagate only within the spherical region of radius R.

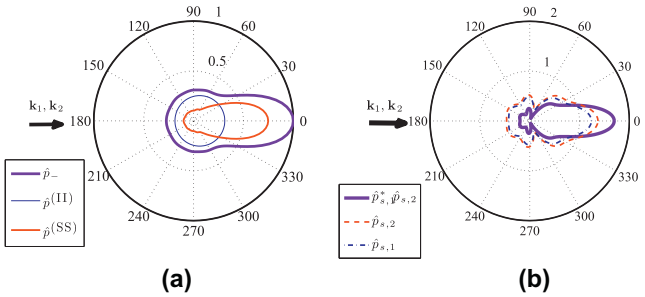

Fig. 3. The directive pattern in the *xz*-plane of (a) the difference-frequency scattered pressure (normalized to maximum value of $|\hat{p}_-|$ which is 0.0823) generated by two collinear plane waves and (b) the linear scattered pressures. The physical parameters used here are $r = 0.1$ m, $R = 2.4$ mm, $a = 1$ mm, $\omega_0/2\pi = 1.5$ MHz, and $\omega_-/2\pi = 100$ kHz. The corresponding size factors are $k_-R = 1$, $k_1R = 14.5$, $k_2R = 15.5$, $k_-a = 0.41$, $k_1a = 6.07$, $k_2a = 6.49$, $k_-r = 41.88$, $k_1r = 607.37$, and $k_2r = 649.26$. The arrows indicate the direction of the incident wavevectors.

quency pressure. The magnitude of this pressure mostly occurs in the forward scattering direction ($\theta = 0^\circ$). We notice that as the radius R of the spherical region increases, the role of $\hat{p}_-^{(\mathrm{II})}$ overcomes the contribution of the scattered-with-scattered interaction. The spatial behavior of $\hat{p}_-^{(\mathrm{SS})}$ resembles that of the linear scattered pressure by the sphere as shown in Fig. 3b.

The dimensionless pressure $\hat{p}_-^{(\mathrm{II})}$ is related to a parametric array whose primary waves are confined in the spherical region of radius R. We can obtain an approximate solution of the parametric array pressure in the farfield, when $\mathbf{r} = r\mathbf{e}_z$ (forward scattering direction $\theta = 0^\circ$). To calculate the parametric array pressure we consider the source term in Eq. (21) as $\mathcal{P} = e^{ik_-r'\cos\theta'}$. Moreover, we approximate the Green's function in the farfield to

$$G = \frac{ik_-(r - r'\cos\theta')}{4\pi r}. \tag{44}$$

Thus, substituting the source term and the Green's function into Eq. (21), we find that the dimensionless parametric array pressure is given by

$$\hat{p}_-^{(\mathrm{PA})} \simeq -\beta k_-^2 R^3 \frac{e^{ik_-r}}{3r}, \quad \theta = 0^\circ. \tag{45}$$

Using the physical parameters of Fig. 3, we find good agreement between this pressure and $\hat{p}_-^{(\mathrm{II})}$, with relative error smaller than 9%. This error might be caused by the presence of the scatterer in the spherical confining region, which is not accounted by Eq. (45).

The directive pattern in the *xz*-plane of the difference-frequency scattered pressure produced by two intersecting plane waves at a right angle ($\theta_2 = 90^\circ$) is displayed in Fig. 4. The component $\hat{p}_-^{(\mathrm{II})}$ corresponds to less 1% of the total pressure and it cannot be seen in this figure. This result is in agreement with early studies which state that two intersecting plane waves at right angle do not produce difference-frequency pressure outside the intersecting region [7]. The term $\hat{p}_-^{(\mathrm{IS,SI})}$ does not contribute significantly to difference-frequency scattered pressure. Thus, $\hat{p}_-^{(\mathrm{SS})}$ is responsible for this pressure. The mainlobes of the difference-frequency scattered pressure lies on the forward scattering directions ($\theta = 0^\circ, 90^\circ$) of each incident wave as depicted in Fig. 4b. Furthermore, these lobes follow the pattern of the linear scattered mainlobes as shown in 4b.

In Fig. 5, we show the directive pattern in the *xz*-plane of the difference-frequency scattered pressure generated in the scattering of two counter-propagating plane waves ($\theta_2 = 180^\circ$). The contributions of $\hat{p}_-^{(\mathrm{II})}$ and $\hat{p}_-^{(\mathrm{IS,SI})}$ are small compared to that from $\hat{p}_-^{(\mathrm{SS})}$. It is known that the counter-propagating waves weakly interact nonlinearly [50]. Thus, the difference-frequency pressure is practically due to $\hat{p}_-^{(\mathrm{SS})}$. The pressure is not symmetric due to a difference in the incident wave frequencies. The difference-frequency pressure follows the behavior of the linear scattered pressures shown in Fig. 5b.

The dependence of the difference-frequency scattered pressure with the radial distance r is exhibited in Fig. 6. The pressure is calculated in the forward scattering direction $\theta = 0^\circ$. In all cases, the main contribution to this pressure comes from $\hat{p}_-^{(\mathrm{SS})}$. Note that according to Eq. (38), the difference-frequency scattered pressure varies as $A_1 r^{-1}\ln r + A_2 r^{-1}$.

The scattered pressure varying with difference-frequency is shown in Fig. 7. The pressure is evaluated at $r = 0.5$ m in the forward scattering direction $\theta = 0^\circ$. In all configurations, the scattered

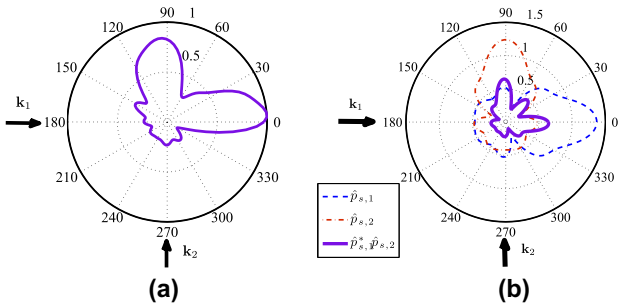

Fig. 4. The directive pattern in the *xz*-plane of (a) the difference-frequency pressure (normalized to 0.0134) produced by two perpendicular plane waves and (b) the linear scattered pressures. The physical parameters used in the evaluation here are the same as those described in Fig. 3. The arrows point to the direction of the incident wavevectors.

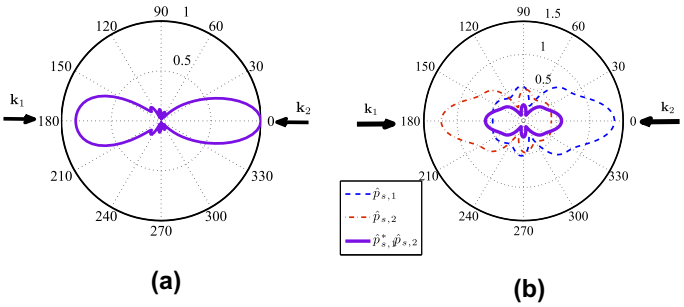

Fig. 5. The directive pattern in the *xz*-plane of (a) the difference-frequency scattered pressure (normalized to 0.0178) due to two counter-propagating plane waves and (b) the linear scattered pressures. The physical parameters used here are the same as those described in Fig. 3. The arrows point to the direction of the incident wavevectors.

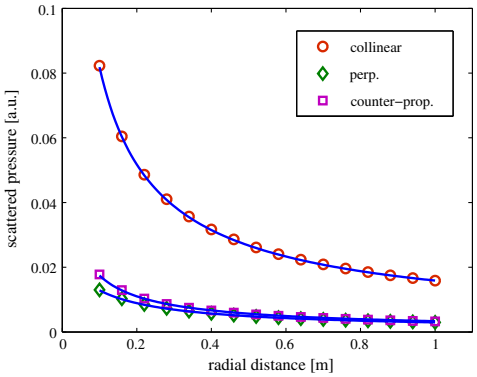

Fig. 6. The (dimensionless) difference-frequency pressure magnitude in the forward scattering direction $\theta = 0^{\circ}$ varying with the radial distance r. The physical parameters used in here are the same as those described in Fig. 3.

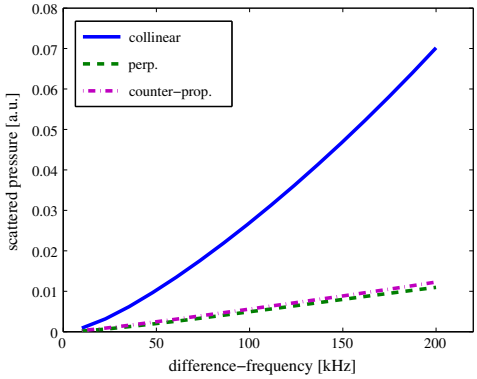

Fig. 7. The (dimensionless) scattered pressure magnitude versus the difference-frequency. The physical parameters used in the evaluation here are the same as those described in Fig. 3.

pressure increases with difference-frequency. The difference-frequency scattered pressures due to the perpendicular and counter-propagating incident plane waves have very close magnitudes. According to Eqs. (25) and (38), the scattered pressure varies with difference-frequency as $\omega_{-} f(\omega_{-})$, where f is a function determined in these equations. Moreover, by referring to Eq. (25) one can show that the difference-frequency scattered pressure diverges when $\omega_{-} \to 2\omega_0$ and $\omega_1 \to 0$. Physically the scattered pressure does not diverge, but it decays due to attenuation instead.

It is worthy to relate our analysis with a previous theoretical study on difference-frequency generation in acoustic scattering [25]. We have tried to draw a direct comparison between this work and the method presented here. Unfortunately, we could not reproduce the reference's results due to the presence of angular singularities in the difference-frequency scattered fields. Therefore, no comparison was possible. Furthermore, we did try to explain the experimental results of difference-frequency generation in the scattering given in Ref. [48]. In this study, a nonlinear scattering experiment was performed involving two collinear beams and a spherical target. The incident waves are generated by a circular flat transducer. Despite the authors claim that the incident beams approach to plane waves, the directive patterns of the linear scattered waves obtained in the experiments do not follow this assumption (see Ref. [49]). Since the scattering does not involve incident plane waves, a direct comparison of our theory (for plane waves) and the experimental results is not reasonable. However, one of the conclusions of Ref. [48] is that the difference-frequency scattered pressure is mostly produced by the incident-with-incident and the scattered-with-scattered interactions. This conclusion is supported by our results.

4. Summary and conclusions

The difference-frequency generation in the scattering of two interacting acoustic waves with an arbitrary wavefront by a rigid sphere was theoretically analyzed. The difference-frequency scattered pressure in the farfield was obtained as a partial-wave series expansion. The amplitude of each partial-wave is given by the interaction function S_l^m, which depends on the observation distance from the scatterer, the beam-shape and scattering coefficients of the primary waves. The developed method was applied to the scattering of two intersecting plane waves located within a spherical region. The directive pattern of the difference-frequency scattered pressure was analyzed in three incident wave configurations: collinear, perpendicular, and counter-propagating. In the collinear arrangement, the incident-with-incident and scattered-with-scattered interactions provide a more prominent contribution to the scattered pressure. In all other configurations, the scattered-

with-scattered interaction prevails over the other interactions. The results show that the scattered pressure increases with difference-frequency. Experimental evidence of this feature was reported in Ref. [19]. Moreover, the scattered pressure was shown to vary with the observation distance as $r^{-1}\ln r$ and $1/r$.

Sound absorption effects in the fluid were not considered. If only compressional waves are assumed to propagate in a weakly viscous fluid, the proposed model can readily accommodate absorption effects by changing the wavenumber $k \to k + i\alpha$, where α is the absorption coefficient. Attenuation may affect the obtained results here in at least one way. Both incident and scattered waves at the fundamental frequencies ω_1 and ω_2 are more attenuated than the difference-frequency scattered wave. Thus, the nonlinear interaction range of the fundamental waves in a viscous fluid is shorter than in a nonviscous fluid. Consequently, a less difference-frequency scattered signal is supposed to be formed in a viscous fluid.

In conclusion, this article presents the difference-frequency generation in nonlinear acoustic scattering of two incident waves with an arbitrary wavefront. This study can help unveil important features of acoustic scattering not dealt with before.

Acknowledgements

This work was supported by Grants 306697/2010-6 CNPq, 477653/2010-3 CNPq, 2163/2009 PNPD-CAPES, and FAPEAL (Brazilian agencies). The authors would like to thank Dr. K. Foote for providing some references.

Appendix A. Surface integral

According to Eq. (19) the surface integral in Eq. (20) is given by

$$I_S = -\frac{(k_- a)^2}{2k_1k_2}\int_\Omega G(r,\theta,\varphi|a,\theta',\varphi')\left.\frac{\partial \mathcal{P}}{\partial r'}\right|_{r'=a} d\Omega'. \tag{A.1}$$

This integral will be estimated for two interacting spherical waves. Thus, the source term $\mathcal{P}$ is given by

$$\mathcal{P}(r') = \frac{e^{ik_- r'}}{k_1k_2r'^2}. \tag{A.2}$$

From Eq. (24) the Green's function becomes

$$G = k_- a\frac{e^{ik_- r}}{r}\sum_{l,m}\frac{(-i)^l}{h_l^{(1)\prime}(k_- a)}Y_l^m(\theta',\varphi')Y_l^m(\theta,\varphi). \tag{A.3}$$

Substituting Eqs. (A.2) and (A.3) into Eq. (A.1), yields

$$I_S = \frac{k_-^3}{2k_1^2k_2^2}(2i + k_- a)\frac{e^{ik_-(r-a)}}{r}. \tag{A.4}$$

Appendix B. Outer volume integral

The outer volume integral reads

$$I_\infty = \beta k_-^2\int_r^\infty\int_\Omega G_\infty(\mathbf{r}|\mathbf{r}')\mathcal{P}(\mathbf{r}')r'^2\,dr'\,d\Omega', \tag{B.1}$$

where the Green's function is given by [46]

$$G_\infty = ik_-\sum_{l,m}\chi_l(k_- r)h_l^{(1)}(k_- r')Y_l^m(\theta,\varphi)Y_l^{m*}(\theta',\varphi'), \tag{B.2}$$

with $a \leqslant r < r'$. We assume that the source term is due the interaction of two spherical waves as given in Eq. (A.2). By substituting Eqs. (A.2) and (B.2) into Eq. (B.1), one finds

$$I_\infty = \frac{\beta k_-}{k_1k_2}\chi_0(k_- r)\int_r^\infty\frac{e^{2ik_- r'}}{r'}dr'. \tag{B.3}$$

After integrating by parts, we obtain

$$I_\infty = \frac{\beta k_-}{k_1k_2}\chi_0(k_- r)\left[\frac{e^{2ik_- r}}{r} + O(r^{-2})\right]. \tag{B.4}$$

Therefore, evaluating $\chi_0(k_- r)$ through the expressions of the spherical functions, we find $I_\infty = O(r^{-2})$.

References

[1] A.L. Thuras, R.T. Jenkins, H.T. O'Neil, Extraneous frequencies generated in air carrying intense sound waves, J. Acoust. Soc. Am. 6 (1935) 173–180.
[2] G.T. Silva, S. Chen, J.F. Greenleaf, M. Fatemi, Dynamic ultrasound radiation force in fluids, Phys. Rev. E 71 (2005) 056617.
[3] G.T. Silva, Dynamic radiation force of acoustic waves on solid elastic spheres, Phys. Rev. E 74 (2006) 026609.
[4] G.T. Silva, S. Chen, L.P. Viana, Parametric amplification of the dynamic radiation force of acoustic waves in fluids, Phys. Rev. Lett. 96 (2006) 234301.
[5] G.T. Silva, M.W. Urban, M. Fatemi, Multifrequency radiation force of acoustic waves in fluids, Physica D 232 (2007) 48–53.
[6] U. Ingard, D.C. Pridmore-Brown, Scattering of sound by sound, J. Acoust. Soc. Am. 28 (1956) 367–369.
[7] P.J. Westervelt, Scattering of sound by sound, J. Acoust. Soc. Am. 29 (1957) 199–203.
[8] J.P. Jones, R.T. Beyer, Scattering of sound by sound, J. Acoust. Soc. Am. 48 (1970) 398–402.
[9] J. Berntsen, J.N. Ttta, S. Ttta, Interaction of sound waves. Part IV: Scattering of sound by sound, J. Acoust. Soc. Am. 86 (1986) 1968–1983.
[10] R.H. Mellen, D.G. Browning, W.L. Konrad, Parametric sonar transmitting array measurements, J. Acoust. Soc. Am. 49 (1971) 932–935.
[11] M. Yoneyama, J. Fujimoto, Y. Kawamo, S. Sasabe, The audio spotlight: an application of nonlinear interaction of sound waves to a new type of loudspeaker design, J. Acoust. Soc. Am. 73 (1983) 1532–1536.
[12] N. Mujica, R. Wunenburger, S. Fauve, Scattering of sound by sound in the vicinity of the liquid–vapor critical point, Phys. Rev. Lett. 90 (2003) 234301.
[13] N. Ichida, T. Sato, M. Linzer, Imaging the nonlinear ultrasonic parameter of a medium, Ultras. Imag. 5 (1983) 295–299.
[14] T. Sato, A. Fukusima, N. Ichida, H. Ishikawa, H. Miwa, Y. Igarashi, T. Shimura, K. Murakami, Nonlinear parameter tomography system using counterpropagating probe and pump waves, Ultras. Imag. 7 (1985) 49–59.
[15] D. Kim, J.F. Greenleaf, C.M. Sehgal, Ultrasonic imaging of the nonlinear parameter B/A: simulation studies to evaluate phase and frequency modulation methods, Ultras. Med. Biol. 16 (1990) 175–181.
[16] D. Zhang, X. Gong, X. Chen, Experimental imaging of the acoustic nonlinearity parameter B/A for biological tissues via a parametric array, Ultras. Med. Biol. 27 (2001) 1359–1366.
[17] M. Fatemi, J.F. Greenleaf, Ultrasound-stimulated vibro-acoustic spectrography, Science 280 (1998) 82–85.
[18] M.W. Urban, G.T. Silva, M. Fatemi, J.F. Greenleaf, Multifrequency vibro-acoustography, IEEE Trans. Med. Imag. 25 (2006) 1284–1295.
[19] G.T. Silva, F.G. Mitri, Difference-frequency generation in vibro-acoustography, Phys. Med. Biol. 56 (2011) 5985–5993.
[20] V.F. Humphrey, C. Murphy, A.H.A. Moustafa, Wideband backscattering measurement using a parametric array, in: Ultrasonics International 87 Conference Proceedings, London, UK, 1987, pp. 265–270.
[21] K.G. Foote, D.T.I. Francis, P.R. Atkins, Calibration sphere for low-frequency parametric sonars, J. Acoust. Soc. Am. 121 (2007) 1482–1490.
[22] L.W. Dean III, Interactions between sound waves, J. Acoust. Soc. Am. 34 (1962) 1039–1044.
[23] J.C. Piquette, A.L.V. Buren, Nonlinear scattering of acoustic waves by vibrating surfaces, J. Acoust. Soc. Am. 76 (1984) 880–889.
[24] L.M. Lyamshev, P.V. Sakov, Nonlinear scattering of sound by a pulsating sphere, Sov. Phys. Acoust. 38 (1992) 50–54.
[25] I.B. Abbasov, N.P. Zagrai, Sphere scattering of nonlinearly interacting acoustic waves, Fluid Dyn. 30 (1995) 158–165.
[26] P.J. Westervelt, Parametric acoustic array, J. Acoust. Soc. Am. 35 (1963) 535–537.
[27] G.T. Silva, Off-axis scattering of an ultrasound Bessel beam by a sphere, IEEE Trans. Ultrason. Ferroelec. Freq. Contr. 58 (2011) 298–304.
[28] F.G. Mitri, G.T. Silva, Off-axial acoustic scattering of a high-order Bessel vortex beam by a rigid sphere, Wave Motion 48 (2011) 392–400.
[29] S. Chen, M. Fatemi, R. Kinnick, J.F. Greenleaf, Comparison of stress field forming methods for vibro-acoustography, IEEE Trans. Ultrason. Ferroelectr. Freq. Control 51 (2004) 313–321.
[30] M.F. Hamilton, D.T. Blackstock, Nonlinear Acoustics, Academic Press, San Diego, CA, 1998. p. 55.
[31] See Ref. [30], p. 54.
[32] See Ref. [30], p. 281.
[33] E.G. Williams, Fourier Acoustics: Sound Radiation and Nearfield Acoustical Holography, Academic Press, Inc., San Diego, CA, 1999. p. 218.
[34] See Ref. [33], p. 206.

[35] L.D. Landau, E.M. Lifshitz, Fluid Mechanics, Pergamon Press, Oxford, United Kingdom, 1987. p. 297.
[36] J.N. Tjotta, S. Tjotta, Interaction of sound waves. Part I: Basic equations and plane waves, J. Acoust. Soc. Am. 82 (1987) 1425–1428.
[37] P.M. Morse, K.U. Ingard, Theoretical Acoustics, Princeton University Press, Princeton, New Jersey, 1986. p. 321.
[38] See Ref. [37], p. 355.
[39] D. Colton, R. Kress, Inverse Acoustic and Electromagnetic Scattering Theory, Springer-Verlag, Berlin, Germany, 1998. p. 63.
[40] H.A. Antosiewicz, in: M. Abramowitz, I.A. Stegun (Eds.), Handbook of Mathematical Functions with Formulas, Graphs, and Mathematical Tables, Dover Publications, New York, NY, 1972, p. 439.
[41] E.W. Weisstein, MathWorld – A Wolfram Web Resource, 2004. <http://mathworld.wolfram.com/Wigner3j-Symbol.html> (viewed 01.12.11).
[42] V. Devanathan, Angular Momentum Techniques in Quantum Mechanics, Springer, New York, NY, 1999. p. 10.
[43] W.J. Wiscombe, Improved Mie scattering algorithms, Appl. Opt. 19 (1980) 1505–1509.
[44] J. Song, W.C. Chew, Error analysis for the truncation of multipole expansion of vector Green's functions, IEEE Microwave Wireless Compon. Lett. 11 (2001) 311–313.
[45] MathWorks Inc. <www.mathworks.com/help/techdoc/ref/quadgk.html> (viewed 10.21.11).
[46] See Ref. [37], p. 354.
[47] C.M. Bender, S.A. Orszag, Advanced Mathematical Methods for Scientists and Engineers: Asymptotic Methods and Perturbation Theory, Springer, New York, NY, 1999. p. 249.
[48] I.B. Abbasov, N.P. Zagrai, An experimental investigation of scattering of nonlinearly interacting plane sound-waves at a sphere, Acoust. Phys. 42 (1996) 267–272.
[49] A.D. Pierce, Acoustics: An Introduction to its Physical Principles and Applications, Acoustical Society of America, Melville, NY, 1989. p. 431.
[50] V. Gusev, H. Bailliet, P. Lotton, M. Bruneau, Interaction of counterpropagating acoustic waves in media with nonlinear dissipation and in hysteretic media, Wave Motion 29 (1999) 211–221.

Bibliography

[1] Hamilton MF, Blackstock DT. Ch. 3. In: PRESS A, editor. Nonlinear Acoustics. San Diego (CA); 1998. .

[2] Crighton DG. Model Equations of Nonlinear Acoustics. Annual Review of Fluid Mechanics. 1979;11:11–33.

[3] Crighton DG. Basic principles of aerodynamic noise generation. Progress in Aerospace Sciences. 1975;16(1):31 – 96.

[4] Whitham GB. On the propagation of weak shock waves. Journal of Fluid Mechanics. 1956;1(3):290 – 318.

[5] Plesset MS, Prosperetti A. Bubble Dynamics and Cavitation. Annual Review of Fluid Mechanics. 1977;9:145 – 185.

[6] Westervelt PJ. Parametric Acoustic Array. The Journal of the Acoustical Society of America. 1963;35(4):535–537.

[7] Szabo TL. Diagnostic Ultrasound Imaging. Press EA, editor. San Diego (CA); 2004.

[8] Richardson JM. Harmonic generation at an unbonded interface-I. Planar interface between semi-infinite elastic media. International Journal of Engineering Science. 1979;17(1):73 – 85.

[9] Beyer RT. Ch. 1. In: Springer-Verlag New York I, editor. Sounds of Our Times. Providence, RI; 1999. .

[10] Thuras AL, Jenkins RT, O'Neil HT. Extraneous Frequencies Generated in Air Carrying Intense Sound Waves. The Journal of the Acoustical Society of America. 1934;6(1):57–57.

[11] Ingard U, Pridmore-Brown DC. Scattering of Sound by Sound. The Journal of the Acoustical Society of America. 1956;28(3):367–369.

[12] Bjorno L. 40 Years of Nonlinear Acoustics. Acta Acustica United With Acustica. 2002;88(5):771–775.

[13] Gong X, Zhang D, Liu J, Wang H, Yan Y, Xu X. Study of acoustic nonlinearity parameter imaging methods in reflection mode for biological tissues. The Journal of the Acoustical Society of America. 2004;116(3):1819–1825.

[14] Yoneyama M, Fujimoto J, Kawamo Y, Sasabe S. The audio spotlight: An application of nonlinear interaction of sound waves to a new type of loudspeaker design. Journal of the Acoustical Society of America. 1983;73(5):1532–1536.

[15] Sato T, Fukusima A, Ichida N, Ishikawa H, Miwa H, Igarashi Y, et al. Nonlinear parameter tomography system using counterprop agating probe and pump waves. Ultrasonic Imaging. 1985;7(1):49 – 59.

[16] Zhang D, fen Gong X, Chen X. Experimental imaging of the acoustic nonlinearity parameter B/A for biological tissues via a parametric array. Ultrasound in Medicine & Biology. 2001;27(10):1359 – 1365.

[17] Fatemi M, Greenleaf JF. Ultrasound-Stimulated Vibro-Acoustic Spectrography. Science. 1998;280(5360):82–85.

[18] Urban MW, Silva GT, Fatemi M, Greenleaf JF. Multifrequency vibro-acoustography. Medical Imaging, IEEE Transactions on. 2006;25(10):1284 – 1295.

[19] Silva GT, Chen S, Greenleaf JF, Fatemi M. Dynamic ultrasound radiation force in fluids. Phys Rev E. 2005;71(5):056617.

[20] Silva GT. Dynamic radiation force of acoustic waves on solid elastic spheres. Phys Rev E. 2006;74(2):026609.

[21] Jackson JD. Ch. 10. In: John Wiley & Sons I, editor. Classical Electrodynamics. University of California, Berkely; 1999. .

[22] Young AT. Rayleigh scattering. Applied Optics. 1981;20(4):533 – 535.

[23] Rayleigh L. On the electromagnetic theory of light. Philosophical Magazine. 1881;.

[24] Rayleigh L. On the incidence of the aerial and electric waves upon small obstacles in the form of ellipsoids of elliptic cylinders and on the passage of electric waves through a circular apperture in a conducting screen. Philosophical Magazine. 1897;40:28–52.

[25] Silva GT, Mitri FG. Analysis of the difference-frequency wave generated by the interaction of two axisymmetric and co-focused ultrasound beams. In: Ultrasonics Symposium, 2008. IUS 2008. IEEE; 2008. p. 1326 –1329.

[26] Aboudi J, Censor D. Scattering of elastic-waves by moving objects. Journal of the Acoustical Society of Americaa. 1972;52(1):203–209.

[27] Piquette JC, Vanburen AL. Nonlinear scattering of acoustic-waves by vibrating surfaces. Journal of the Acoustical Society of Americaa. 1984;76(3):880–889.

[28] Abbasov IB, ZagraiI NP. Scattering of Interacting Plane-Waves by a Sphere. Acoustical Physics. 1994;40(4):473–479.

[29] Abbasov IB. Study of the scattering of nonlinearly interacting plane acoustic waves by an elongated spheroid. Journal of Sound and Vibration. 2008;309(1-2):52 – 62.

[30] Lighthill MJ. On sound generated aerodynamically - I. General Theory. Proceedings of the Royal Society of London Series A, Mathematical and Physics Sciences. 1952;211(1107):564–587.

[31] Tjotta JN, Tjotta S. Interaction of sound waves. Part I: Basic equations and plane waves. The Journal of the Acoustical Society of America. 1987;82(4):1425–1428.

[32] Rossing TD. Ch. 8. In: Springer, editor. Handbook of Acoustics. Stanford, CA; 2007. .

[33] Williams EG. Fourier Acoustics. Sound Radiation and Nearfield Acoustical Holography. PRESS A, editor. San Diego (CA); 1999.

[34] Abramowitz M, Stegun IA. Handbook of Mathematical Functions with Formulas, Graphs, and Mathematical Tables. Dover, editor. New York; 1972.

[35] Wigner 3j-Symbol. MathWorld–A Wolfram Web Resource; [cited 2011 June 07]. Available from: http://mathworld.wolfram.com/Wigner3j-Symbol.html.

[36] Devanathan V. Angular Momentum Techniques in Quantum Mechanics. Springer, editor. New York; 1999.

[37] Research W. Mathematica. Version 7.0 ed. Champaign, Illinois: Wolfram Research; 2010.

[38] Exponential Integral. MathWorld–A Wolfram Web Resource; [cited 2011 June 08]. Available from: http://mathworld.wolfram.com/ExponentialIntegral.html.

[39] Ishimaru A. Wave Propagation and Scattering in Random Media. Marketing IP, editor. New York; 1997.

[40] Goldberg BB. Presidential message in WFUMB. Ultrasound in Medicine and Biology. 1997;23(6):A1–A2.

[41] Wells PNT. Ultrasound imaging of the human body. Reports on Progress in Physics. 1999;62(5):671–722.

[42] Gao L, Parker KJ, Lerner RM, Levinson SF. Imaging of the elastic properties of tissue–A review. Ultrasound in Medicine & Biology. 1996;22(8):959 – 977.

[43] Feynman RP, Leighton RB, Sands M. Ch. 48. In: Addison-Wesley Publish-

ing Company M Inc, editor. The Feynman Lectures on Physics II. Palo Alto - London; 1964. .

[44] Fatemi M, Greenleaf JF. Vibro-acoustography: An imaging modality based on ultrasound-stimulated acoustic emission. Proceedings of the National Academy of Sciences of the United States of America. 1999;96(12):6603–6608.

[45] Pierce AD. Acoustics: An Introduction To Its Physical Principles and Applications. ASA, editor. Melville (NY): ASA; 1989.

[46] Chen S, Silva GT, Kinnick RR, Greenleaf JF, Fatemi M. Measurement of dynamic and static radiation force on a sphere. Phys Rev E. 2005;71(5):056618.

[47] Colton D, Kress R. Inverse Acoustic and Electromagnetic Scattering Theory. Springer-Verlag, editor. Berlin; 1998.

[48] Morse PM, Ingard KU. Theoretical Acoustics. Princeton, New Jersey: Princeton University Press; 1986.